Aus der Medizinischen Klinik mit Schwerpunkt Hämatologie, Onkologie und Tumorimmunologie (Campus Virchow-Klinikum)
der Medizinischen Fakultät Charité – Universitätsmedizin Berlin

DISSERTATION

Antibody-mediated direct killing and senolytic capacity of two distinct anti-CD20 monoclonal antibodies in human diffuse large B-cell lymphoma cell lines

Antikörper-vermittelte direkte Abtötung und senolytische Kapazität zwei monoklonaler Anti-CD20-Antikörper in humanen diffus großzelligen B-Zell-Lymphom-Zelllinien

zur Erlangung des akademischen Grades
Doctor medicinae (Dr. med.)

vorgelegt der Medizinischen Fakultät
Charité – Universitätsmedizin Berlin

von

Xinxin Sun
aus Zhengzhou, China

Datum der Promotion: 26. Juni 2022

Table of Contents

List of Figures

List of Tables

List of Abbreviations

Ab	antibody
ABC	Activated B-cell
ADCC	Antibody dependent cell cytotoxicity
ADCP	Antibody dependent cellular phagocytosis
ADR	Adriamycin
APS	Ammonium persulfate
ASH	American Society of Hematology
ATP	Adenosine triphosphate
BCA	Bicinchoninic acid
BSA	Bovine serum albumin
C12FDG	12-carbon fluorescein di-β-D-galactopyranoside
CCFs	Cytoplasmic chromatin fragments
CCL2	Chemokine ligand 2
CDC	Complement dependent cytotoxicity
CDK	Cyclin-dependent kinases
cDNA	Complementary DNA
cGAS	Cyclic GMP-AMP synthase
Cyclic GMP-AMP	Cyclic guanosine monophosphate–adenosine monophosphate
CHOP	Cyclophosphamide plus hydroxydaunorubicin plus vincristine sulfate plus prednisone
COO	Cell of origin
CR	Complete response
DDR	DNA damage response
DNA	Deoxyribonucleic acid
DLBCL	Diffuse large B-cell lymphoma
DMSO	Dimethyl sulfoxide
ECM	Extracellular matrix
FBS	Fetal bovine serum
FC	Fragment crystallizable

FDG	Fluorescein di-β-D-galactopyranoside
FL	Follicular lymphoma
GAPDH	Glyceraldehyde 3-phosphate dehydrogenase
GCB	Germinal center B-cell
H3K9me3	Histone 3 lysine 9 trimethylation
HP1	Heterochromatin Protein 1
IHC	Immunohistochemistry
IgG	Immunoglobulin class G
IL1α	Interleukin 1α
IL-6	Interleukin 6
IMDM	Iscove's modified Eagle's medium
kD	Kilodalton
LCD	Lysosomal cell death
LMP	Lysosomal membrane permeabilization
LPS	Linear prediction score
mAb	Monoclonal antibody
MHC	Major histocompatibility complex
ml	Milliliter
MOMP	Mitochondrial outer membrane permeabilization
mRNA	Messenger RNA
NF-κB	Nuclear factor kappa-light-chain-enhancer of activated B cells
NHL	Non-Hodgkin lymphoma
O-CHOP	Obinutuzumab plus CHOP
OIS	Oncogene-induced senescence
OS	Overall survival
PBS	Dulbecco’s phosphate buffered saline
PCR	Polymerase chain reaction
PFA	Paraformaldehyde
PFS	Progression-free survival
PMTs	Photomultiplier tubes

qRT-PCR	Quantitative Real Time-PCR
RB	Retinoblastoma tumor suppressor gene
RNA	Ribonucleic acid
ROS	Reactive oxygen species
R-CHOP	Rituximab plus CHOP
RT	Reverse transcription
Sa-β-gal	Senescence-associated beta-galactosidase
SAHF	Senescence-associated heterochromatin foci
SAS	senescence-associated stemness
SASP	Senescence-associated secretory phenotype
SD	Standard deviation
SDS	Sodium dodecyl sulfate
STING	Stimulator of interferon genes
t+	t(14,18)-positive
t-	t(14,18)-negative
TF	Transcription factors
TGF-β	Transforming growth factor beta
TIS	Therapy induced senescence
TM	Transmembrane
Ut	Untreated
V	Voltage
WB	Western blot
γ H2AX	phosphorylated form of H2A histone family member X
µg	Microgram
µL	Microliter

Abstract (English)

Introduction

The type II anti-CD20 monoclonal antibody Obinutuzumab (O) combined with cyclophosphamide, adriamycin, vincristine, and prednisone, also known as O-CHOP, didn't show superiority over type I antibody Rituximab (R) combined with CHOP (R-CHOP) in the Phase III GOYA clinical trial[1] which included 1,418 diffuse large B-cell lymphoma (DLBCL) patients. However, further analysis of the cohort by the cell of origin identified 25% of the overall population as a strong germinal center B-cell (GCB) subgroup, characterized with a higher t(14,18)(q32;q21) translocation incidence rate, in which O-CHOP demonstrated superiority to R-CHOP. Our previous work reported that primary GCB-like Eμ-myc mouse lymphoma samples transduced with Bcl2 are prone to senescence. It has been long known that chemotherapy may result in cellular senescence, and more recent work has indicated senescence to potentially have a detrimental effect, to some extent, due to senescence-associated secretory phenotype (SASP) and senescence associated stemness (SAS). However, it is not known whether senescence underlies the differential O-CHOP vs. R-CHOP treatment efficacy in strong GCB patients. As a possible mechanism, I explored the Ab-mediated direct killing of senescent human DLBCL cells.

Methods

DLBCL cell lines with or without t(14,18) (t+ or t-) were treated with Obinutuzumab or Rituximab in different concentrations. The viable cell number was measured by flow cytometry. These cell lines were first treated with ADR and induced to enter cellular senescence. Senescence-associated beta-galactosidase (SA-β-gal) activity, SASP, and SAS gene expression were evaluated for confirmation of the senescent status. Next, the senolytic capability of Obinutzumab and Rituximab was tested for Ab-mediated direct killing of the senescent cells. The senolytic result was verified by detecting senescence markers, e.g., detecting H3K9me3, p16, and γH2AX by western blot. Further mechanisms of how the senescent cells were killed were monitored by lyso-sensor tracking lysosomal pH changes as a part of the senolytic process. Cleaved Caspase-3 was used as an indicator of apoptosis during the senolytic process.

Results

In Ab-mediated direct killing assay, Obinutuzumab showed stronger efficacy than Rituximab in both t+ and t- cell lines. Obinutuzumab also exerted higher cytotoxcity in the t+ subgroup as compared to the t- subgroup. ADR-induced senescence in DLBCL cell lines induced higher SA-β-gal activity and SASP as well as SAS gene expression. In particular, Obinutuzumab had higher senolytic capability in the t+ cell lines. The senolytic process of Obinutuzumab in the t+ was associated with lysosome status.

Conclusions

Obinutuzumab had higher Ab-mediated direct killing and senolytic capability than Rituximab *in vitro*. These findings might explain, at least in part, why the subgroup of strong GCB patients presented with longer progression-free survival after O-CHOP treatment in the GOYA clinical trial.

Abstract (German)

Einleitung

In der Phase III-Studie „GOYA“, an der 1.418 Patientinnen und Patienten mit diffus großzelligem B-Zell-Lymphom (DLBCL) teilnahmen, zeigte der monoklonale Typ-II-Anti-CD20-Antikörper Obinutuzumab (O) in Kombination mit Cyclophosphamid, Adriamycin, Vincristin und Prednison (O-CHOP) keine Überlegenheit gegenüber dem Typ-I-Antikörper Rituxmab (R) in Kombination mit CHOP (R-CHOP). Eine weitere Analyse der Kohorte hinsichtlich der Ursprungszelle identifizierte jedoch 25% der Gesamtpopulation als eine starke Keimzentrums-B-Zell (GCB)-Subgruppe, die durch eine höhere t(14,18)(q32;q21)-Translokationsrate charakterisiert war und bei der O-CHOP eine Überlegenheit gegenüber R-CHOP zeigte. Vorherige Arbeiten unserer Gruppe zeigten, dass GCB-ähnliche primäre Eμ-myc-Maus-Lymphome, die mit Bcl2 transduziert wurden, anfällig für Seneszenz sind. Es ist bereits bekannt, dass eine Chemotherapie zu zellulärer Seneszenz führen kann, wobei jüngere Arbeiten zeigen, dass Seneszenz aufgrund des Seneszenz-assoziierten sekretorischen Phänotyps (SASP) und der Seneszenz-assoziierten Stammzell-Reprogrammierung (SAS) auch eine schädliche Wirkung entfalten kann. Inwiefern Seneszenz an der unterschiedlichen Wirksamkeit von O-CHOP- vs. R-CHOP in der starken GCB-Subgruppe beteiligt sein könnte, ist bisher nicht bekannt. In dieser Arbeit habe ich den möglichen Mechanismus der Antikörper (Ab)-vermittelten direkten abtötenden Wirkung auf seneszente humane DLBCL-Zelllinien in *vitro* untersucht.

Methoden

DLBCL-Zelllinien mit oder ohne t(14,18)-Translokation (t+ oder t-) wurden in verschiedenen Konzentrationen mit O oder R behandelt. Die Anzahl viabler Zellen wurde mittels Durchflusszytometrie gemessen. Zunächst erfolgte die Behandlung der Zelllinien mit Adriamycin, um zelluläre Seneszenz zu induzieren. Die Aktivität der Seneszenz-assoziierten beta-Galaktosidase (SA-β-gal) sowie die Expression von SASP- und SAS-Genen wurden zur Bestätigung der Seneszenzauslösung evaluiert. Als nächstes wurde die senolytische Fähigkeit von O und R auf die Ab-vermittelte direkte Abtötung der seneszenten Zellen getestet. Das senolytische

Ergebnis wurde durch den Nachweis von Seneszenz-Markern wie H3K9me3, p16 und γH2AX durch Western Blot verifiziert. Weitere Mechanismen der Abtötung seneszenter Zellen wurde mittels Überwachung lysosomaler pH-Veränderungen als Teil des senolytischen Prozesses untersucht. Geteilte Caspase-3 wurde als Apoptoseindikator während des senolytischen Prozesses verwendet.

Ergebnisse

Hinsichtlich der Ab-vermittelten direkten Zytotoxizität in den t+ - und t- -Zelllinien zeigte O in beiden Untergruppen eine stärkere Wirksamkeit als R, wobei O in der t+ -Untergruppe stärker zytotoxisch als in der t+ -Untergruppe wirkte. Adriamycin-induzierte Seneszenz zeichnete sich in DLBCL-Zelllinien durch eine hohe SA-β-Gal-Aktivität und eine erhöhte SASP- und SAS-Genexpression aus. Im Speziellen zeigte O eine höhere senolytische Fähigkeit in den t+ -Zelllinien. Der senolytische Prozess von O war in den t+-Zelllinien mit dem Lysosomenstatus assoziiert.

Schlussfolgerung

O hat eine höhere Wirksamkeit hinsichtlich der Ab-vermittelte direkten Abtötung und eine höhere senolytische Fähigkeit als R. Dies könnte einer der Gründe dafür sein, dass Patientinnen und Patienten mit starker GCB-Subgruppe in der GOYA-Studie durch die O-CHOP-Behandlung ein längeres progressfreies Überleben erzielten.

1 Introduction

1.1 Diffuse large B-cell lymphoma (DLBCL) and its subtypes

Lymphoma is blood cancer from lymphocytes consisting of 90% non-Hodgkin lymphoma (NHL) and 10% Hodgkin lymphoma[2,3]. The annual incidence rate of NHL is 16.1 per 100,000 persons in men and 11.7 in women in Germany as of 2020 (Robert Koch Institute)[4]. DLBCL is the most common type of NHL originating from B lymphocytes.[3]

With the development of the newest technologies probing patient material at the level of individual gene sequence and expression level, the histopathological classification of diseases are being updated with molecular subgroups. In DLBCL, several subgroup classifiers have been established. The most well-known is the classification by cell of origin (COO), which defines three subtypes based on the gene expression pattern related to normally developing B lymphocytes[5]: Germinal center B-cell (GCB), activated B-cell (ABC), and the rest which are unclassifiable. Additionally, Lymph2Cx assay is typically for fixed, paraffin-embedded tissue of COO. By applying simple linear regression and Bayes' theorem algorithm on the COO, Wright and colleagues set up a linear prediction score (LPS) platform with 20 genes to predict three different subgroups irrespective of the gene expression profiling method.[6] From genetic features, recurrent t(14,18) translocations are virtually exclusively found in the GCB-DLBCL subgroup, while ABC-DLBCLs have recurrent trisomy 3 and deletion of the CDKN2A (inhibitor of kinase 4A-alternative reading frame) locus as well as activation of the nuclear factor kappa-light-chain-enhancer of activated B cells (NF-κB) pathway.[7] The COO subgroups of DLBCL have a prognostic value regarding clinical chemotherapy response and non-GCB-DLBCLs (ABC and unclassifiable) have an inferior survival rate than GCB-DLBCLs when treated with standard R-CHOP.[5]

Another classifier[8] is based on protein level molecular features by immunohistochemistry (IHC), by which double expressor lymphomas have overexpression of c-MYC (≥ 40% incidence rate) and BCL2 (≥ 50% incidence rate) due to chromosome rearrangement. Double-hit- or triple-hit lymphomas have a genetic rearrangement in c-MYC in addition to BCL2 and/or BCL6. There is overlap between the COO and IHC molecular features classifier. Double expressor lymphoma,

which is associated with high MYC and BCL2 expression, occurs mainly in the ABC subtypes. Alternatively, double-hit or triple-hit lymphoma, which has concurrent translocation of MYC and BCL2, is found more in the GCB subtype.[9] The third classifier is based on recurrent mutations revealed by whole exome sequencing and defines four different subgroups: MCD (co-occurrence of MYD88 and CD79), BN2 (BCL6 fusion and NOTCH2), N1 (NOTCH1), and EZB (EZH2 and BCL2 translocation).[10] The fourth classifier is based on somatic copy number alterations, recurrent mutations, and low-frequency genetic alterations, and identifies five clusters which include C1 (marginal zone origin), C3 (poor risk GCB-DLBCLs with BCL2SVs and alterations of PTEN and epigenetic enzymes), C4 (good-risk GCB-DLBCLs with distinct alterations in BCR/PI3K, JAK/STAT and BRAF pathway components as well as multiple histones), C2 (COO-independent group), and C5 (frequent BCL2 gain, concordant MYD88/CD79B mutations).[11] Generally speaking these classifiers have both advantages and limitations. While they promote the understanding of the pathogenic mechanisms of cancer, it is difficult to apply them in prospective assessment of the patients to give guidance for the treatment. More efforts are needed to set up new ones that could be easily and efficiently implemented in clinics to promote precision diagnosis and treatment for the patients.

1.2 DLBCL therapy and monoclonal antibody (mAb)

For last few decades, DLBCL has been treated by combination chemotherapy, which improved overall survival (OS) of patients substantially. For example, in early 1990s the classical combination strategy CHOP had a CR rate of around 40%-50%.[12] But it was still far from curable at that time and a shortage of traditional chemotherapy, which had no clear target and serious side effects, raised the need for new methods. One of them was immunotherapy. Anti-CD20 therapeutic monoclonal antibody, Rituximab (R), has been the most widely used and successful therapy in clinics since the late 1990s. Rituximab is produced in the hybridoma cell line as a chimeric molecule, constructed by ligating the murine variable region of the anti-CD20 antibody with the human IgG constant region. It targets CD20 antigen and is recommended for the treatment of nearly all B cell NHLs and commonly given in combination with chemotherapy. CHOP combined

with Rituximab (R-CHOP) is the first line therapy for DLBCL resulting in significantly increased progression-free survival (PFS) and significantly longer overall survival (OS) than CHOP only.[13]

Despite 20 years of clinical use, we have only touched a small part of the mechanism behind the therapeutic monoclonal antibody. Four different mechanisms have been suggested about how therapeutic mAbs may kill tumor cells: antibody dependent cell cytotoxicity (ADCC), antibody dependent cellular phagocytosis (ADCP), Ab-mediated direct killing, and complement dependent cytotoxicity (CDC).[14] However, for the Ab-mediated direct killing, research has seldom been performed. Antibody binding may block the receptor-ligand interactions, as, for example, therapeutic antibodies against epidermal growth factor receptor (EGFR) or as human epidermal growth factor receptor 2 (Her-2) may hamper intracellular proliferating signal. In the case of Rituximab, this scenario does not apply, because CD20 has no enzymatic function and no natural ligand has been identified so far. It is a tetra-transmembrane protein which has an intracellular N- and C-terminal region and two extracellular loops. The two loops are partly targeted by current therapeutic mAbs.[15] It is proposed as calcium channel. Rituximab binding induced translocation of CD20 into lipid raft is important for calcium influx.[16] Evidence about more signals passing down into the nucleus was published by Stephan Mathas and colleagues, stating that it was correlated with fast up-regulation of proapoptotic protein Bax and was thus inducing apoptosis in human surface IgM-positive Burkitt's lymphoma cell lines as well as more mature B-cell lymphoma cell lines.[17]

Even though anti-CD20 monoclonal antibody Rituximab has been the most successful immunotherapeutic that is applied for DLBCL patients, not all patients could get the benefit, as the disease would go into relapse and gain resistance to Rituximab. Therefore, an improved version of it, the manipulated type II antibody Obinutuzumab (O), was developed. Obinutuzumab has a partial overlap of the CD20 epitope with Rituximab. The elbow angle of Obinutuzumab is 167, which is different from that of Rituximab (elbow angle 140), and has a big influence on the affinity of the epitope and paratope binding. Another difference is that Obinutuzumab is glycoengineered with the fucose removed from Fc region.[18] It has been shown that Obinutuzumab increased ADCC and Ab-mediated direct killing, but lowered CDC compare to Rituximab.[19] However, the

mechanisms behind it are not well studied. Regarding Ab-mediated direct killing by Obinutuzumab, one group observed cathepsin B-related lysosomal cell death once the antibody binding on the antigen induced aggregation.[20] However, a separate group challenged this hypothesis because of the unspecific binding of anti-cathepsin B antibodies, resulting in a false positive result when repeating the same assay.[21]

1.3 Therapy-induced senescence and senolytic effect

Cellular senescence is a stable cell-cycle arrest status induced by cellular stress, with features including cell cycle halt, morphological and metabolic change, formation of senescence-associated heterochromatin foci (SAHF) with gene expression profile alteration, and senescence-associated secretory phenotype (SASP) as well as senescence-associated stemness (SAS).[22,23] Based on different factors that initiate the process, there is replicative senescence, oncogene-induced senescence (OIS), and therapy-induced senescence (TIS). Replicative senescence (also termed as Hayflick limit) was first experimentally discovered in non-malignant cells in the early 1960s and occurs due to telomeres progressively shortening in every cell division.[24] OIS happens as the cellular response to oncogenic signaling, a safeguard mechanism to stop the transformation to malignant cells in a potent cell autonomous manner.[25] TIS is triggered by DNA damage (e.g. radiation, chemotherapy, oxidative stress, and genotoxic stress) and involves p53/p21 and p16/pRb pathways as a part of DNA damage response (DDR).[26]

Cancer cells typically have the ability to evade the Hayflick limit and therefore have unlimited proliferation capability.[27] Controlling tumor cell proliferation and finally eliminating them become the main target of saving human life when patients get any type of tumors. Therapy reagents like chemotherapeutics have to be toxic for these fast-growing malignant cells. Upon treatment, cumulative DNA damage in the tumor cells first triggers DDR pathways. Apoptosis is induced when the cumulative damage is too serious to be tolerable for the cell, preventing damaged DNA from passing through new generations. If the damage is not lethal but cannot be repaired instantly, the cell will stop the cell cycle, under yet-to-be elucidated circumstances and even enter senescence as a terminal cell-cycle arrest condition. Genomic reorganization and SAHF formation

are not considered to reflect an (aberrant) DNA repair mechanism. The combination of DNA repairment, chromatin re-organization and SAHF, neighbor cell communication as SASP, and the immune system response generates a new tumor environment. This is a particularly complicated process and it can be beneficial or detrimental - so far it is not clear how this direction is determined. Differently from replicative senescence, evidence shows that these TIS cells might occasionally re-enter the cell cycle once chemotherapeutics are removed, with either similar pre-senescent status or gaining more malignant features. Work by our laboratory has demonstrated that senescent cells undergo a reprogramming process during defending against the damage, and by re-entering the cell cycle, they may gain more stemness features.[23] This might be a possible mechanism of how patients would go into relapse and become more difficult to be cured. Therefore, killing senescent cells (senolysis) after therapy aims to eliminate these potent senescent cells with reprogrammed stemness. A lot of agents like Navitoclax were found to have senolytic capability. Rituximab and Obinutuzumab have Ab-mediated direct killing of tumor cells, and in addition, Rituximab was shown to exert pro-senescent capacity as well.[28] However, it is not known whether Rituximab and Obinutuzumab also have senolytic capability.

1.4 Lysosomal cell death and apoptosis

Cancer treatment aims to decrease tumor burden completely, and to avoid relapse in the future so as to finally cure the patients. There are different ways of tumor cell death under different kinds of treatment. Elucidating the type of cell death tries to characterize the genetic molecular pathway that is propagated inside the cell and the living environment that is affected outside the cell. As programmed cell death, apoptosis has processes including blebbing, cell shrinkage, nuclear fragmentation, chromatin condensation, chromosomal DNA fragmentation, and global mRNA decay. The apoptotic bodies could be engulfed by phagocytic cells and there is no damage to the surrounding cells. There are intrinsic and extrinsic apoptosis types. Both of them need caspases, and mainly caspase-3, as executioners.[29] Lysosomal cell death (LCD) was first presented by Christian de Duve in the 1980s[30] and was later found to be associated with lysosomal membrane

permeabilization (LMP) and followed by the release of lysosomal contents, for example, the cathepsin family, to the cytoplasm.[31] The upstream molecular mechanism of LMP is not fully elucidated. ROS might play a role in terms of activating lysosomal Ca^{2+} channels.[32] Interestingly, there might be some interconnection between apoptosis and LCD. It has been shown that intrinsic apoptosis signalling induces mitochondrial outer membrane permeabilization (MOMP) followed by LMP. [33] However, LCD without MOMP and caspases is possible, and may also not involve morphology changes like apoptosis. [34]

2 Hypothesis

The phase III GOYA[1] clinical trial involved 1,418 DLBCL patients, and aimed to compare two therapy strategies, namely Obinutuzumab (GA101, G) plus CHOP (O-CHOP; in GOYA it was termed G-CHOP) and Rituximab plus CHOP (R-CHOP). The results found no difference between O-CHOP and R-CHOP treatment for all patients both in the PFS rate and OS rate. Data are shown in Table 1. The team then divided the patient cohort by the COO classification method into GCB, ABC, and unclassified subgroups, but still could not find a superiority of O-CHOP to R-CHOP in all subgroups. Data are shown in Table 2. Note that in GCB subgroup, the hazard ratio (HR) was 0.72 with a 95% confidence interval (CI) from 0.50 to 1.01.

Outcome	Population(n)	HR	95% CI	p-value
PFS	R-CHOP(n=712) vs O-CHOP(n=706)	0.92	0.76-1.11	0.3868
OS	R-CHOP(n=712) vs O-CHOP(n=706)	0.78	0.78-1.28	0.9982

Table 1. GOYA trial outcomes of PFS and OS.

Subtype	Population(n)	HR	95% CI
GCB	R-CHOP(n=269) vs O-CHOP(n=271)	0.72	0.50-1.01
ABC	R-CHOP(n=118) vs O-CHOP(n=125)	0.86	0.57-1.29
Unclassified	R-CHOP(n=75) vs O-CHOP(n=75)	1.02	0.60-1.75

Table 2. PFS of three subtypes of DLBCL in GOYA trial.

The GALLIUM clinical trial[35] had the same setup comparing O-CHOP with R-CHOP on follicular lymphoma (FL) patients. Here, the O-CHOP treatment had a longer PFS rate than the R-CHOP

treatment. There is no difference in the OS rate between the two different treatments. Data are shown in Table 3.

Outcome	Population(n)	HR	95% CI	p-value
PFS	R-CHOP(n=601) vs O-CHOP(n=601)	0.66	0.51-0.85	0.001
OS	R-CHOP(n=601) vs O-CHOP(n=601)	0.75	0.49-1.17	0.21

Table 3. GALLIUM trial outcomes of PFS and OS.

A similar trend was observed in the GOYA GCB subgroup data when comparing it with GALLIUM PFS rate data. Sequencing by Morin and colleagues aiming to find mutations in DLBCL and FL patients[36] revealed that there were some overlapping gene mutation patterns (co-occurrence and mutual exclusion) between GCB enrichment and FL patients (Figure 1A).

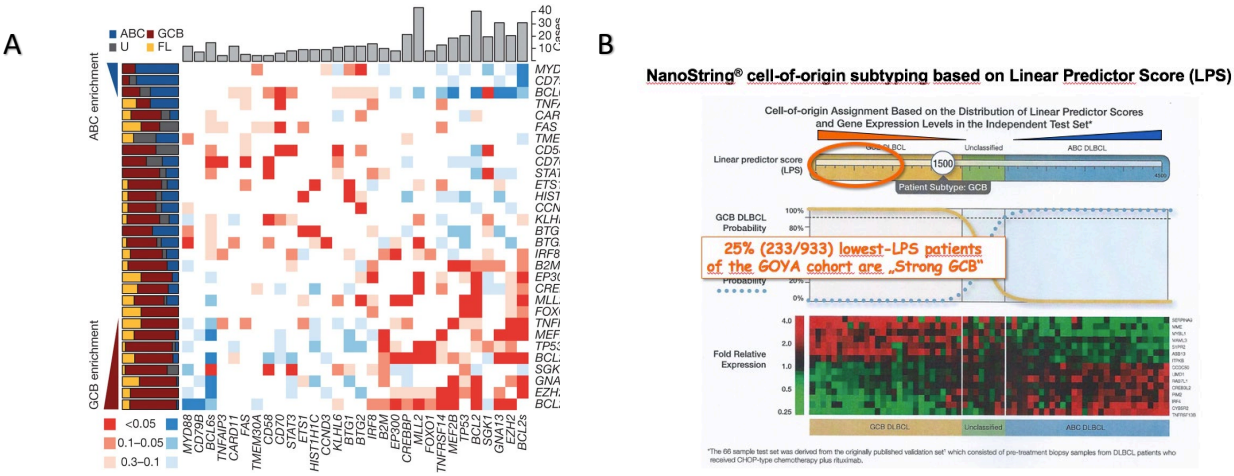

Figure 1. (A) Gene mutations in DLBCL and FL from Morin-RD and colleagues in Nature 2011[36]. (B) LPS score platform with associated GOYA data from Oestergaard-MZ, Lenz-G and colleagues, ASH 2017 #1543.

The GOYA team made a further analysis of their patients by applying the LPS platform. Each of the patients got a score based on a 20 gene expression pattern (Figure 1B). They named the 25% (233/933) lowest LPS score patients as strong GCBs, and found that these strong GCBs patients exhibited FL reminiscent characteristics. For example, FL-typical t(14,18)(q32;q21) translocation has a 85% incidence rate in FL. This translocation incidence rate in strong GCBs is 52%, whereas it is 19% in weak GCBs. FL typical mutations like CREBBP, EZH2, TNFRSF14, EP300, and MEF2B have happened more in strong GCBs than in weak GCBs. Comparing this again with the

two treatment strategies, strong GCBs patients have a significantly longer PFS rate with O-CHOP than R-CHOP (Table 4). These data were demonstrated to the American Society of Hematology (ASH) in 2016 by Oestergaard and colleagues, and were recently published in part.[37] In essence, these findings allow the approximation of Nanostring Lymph2Cx-classified "strong GCB" patients by a positive t(14;18) translocation status.

Outcome	Population(n)	HR	95% CI	p-value
PFS	R-CHOP(n=121) vs O-CHOP(n=112)	0.33	0.18-0.63	0.0007
OS	R-CHOP(n=121) vs O-CHOP(n=112)	0.41	0.20-0.87	0.019

Table 4. Outcome of PFS and OS in strong GCBs in GOYA trial.

Outcome	Population(n)	HR	95% CI	p-value
PFS	R-CHOP(n=341) vs O-CHOP(n=359)	0.99	0.76-1.26	0.9117
OS	R-CHOP(n=341) vs O-CHOP(n=359)	1.10	0.79-1.53	0.582

Table 5. Outcome of PFS and OS in all other patients in GOYA trial.

In previous work by our laboratory[38], it was reported that primary GCB-like Eμ-myc mouse lymphoma samples transduced with Bcl2 are prone to senescence, which was dependent on the NF-κB pathway. They further analyzed human patient data and found Bcl2-high GCB DLBCL with NF-κB high expression correlated with a longer PFS rate than NF-κB low expression, with the reasons being that a senescence-promoting NF-κB targeted cascade would play a tumor-restraining role. This is a supportive standpoint for senescence in the tumor. Subsequent work by our group[23] revealed a more broadly detrimental aspect of SAS, in that therapy induced, senescence associated reprogramming could promote cancer stemness, which leads to more aggressive relapses in aggressive lymphoma, acute lymphoblastic leukemia, and acute myeloid leukemia models with a supportive, consistent result in human colorectal cancer and melanomas

cell lines as well as primary human hematological malignancies. There is still an argument as to whether senescence would be an ally or an enemy in cancer treatment, as well as whether senescence also plays a role in the scenario whereby O-CHOP benefits strong GCB patients. The question arises as to how the process is conducted. ADR-induced senescence in cancer therapy has been reported on in the literature.[39] Chemotherapy in O-CHOP includes ADR, since known senescent cells always develop increased lysosomal content to hydrolysis misfolded proteins due to DNA damage. Additionally, Obinutuzumab might have a lysosome induced cell death manner according to a published paper on Ab-mediated direct killing.[20] It is possible that there is an interaction between chemotherapeutics and mAb in the combination strategy. Using this clue, my thesis project explored the direction of the Ab-mediated direct killing and senolytic capability of Obinutuzumab by comparing it with Rituximab in human DLBCL cell lines with and without t(14,18), i.e., the activation and overexpression of Bcl2, and the role that senescence would play inside.

The hypothesis of the project was that Obinutuzumab may preferentially kill senescent cells by lysosomal changes in DLBCL cell lines with t(14,18).

3 Materials and methods

3.1 Materials

3.1.1 Chemicals and reagents

Name	Manufacturer
2-Propanol	Roth
30% Acrylamide/Bis-acrylamide	Roth
4% Histofix	Roth
Adriamycin (Doxorubicin, ADR), 2mg/ml	Charité pharmacy
Ammonium persulfate (APS)	Roth
Bovine serum albumin (BSA)	Sigma
DAPI	Sigma
Dimethyl sulfoxide (DMSO)	Merck
Ethanol, absolute	Roth
Fetal bovine serum (FBS)	Sigma
Glutaraldehyde	Roth
Glycerol	Roth
Glycine	Roth
Hydrochloric Acid, Hcl	Merck
Iscove's modified Eagle's medium	Gibco
L-glutamine(powder)	Biochrom
Magnesium chloride (MgCl2.6H2O)	Roth
Methanol	Roth
Paraformaldehyde	Sigma
Penicillin streptomycin	Biochrom

Name	Manufacturer
Potassium ferricyanide(K3Fe(CN)6)	Sigma
Propidium iodide	Sigma
RPMI 1640	Gibco
Sodium dodecyl sulfate (SDS)	Roth
Sodium chloride (Nacl)	Roth
Sodium hydroxide (NaOH)	Roth
Tris base	Invitrogen
TEMED	Sigma
TRIZOL	Invitrogen
Trypan blue solution	Sigma
Trypsin	Biochrom
Tween 20	Roth
Whatman filter paper	Roth
X-gal	Roth

3.1.2 Equipment

Equipment name	Manufacturer
Cell culture dishes and falcons	TPP
Cell culture incubator	Ibs tecnomara
Centrifuge	Thermo Fisher
Chemiluminescence detector	FUJIFILM LAS4000
Cryotubes	Sefar
Guava easyCyte™ 12HT Systems	Luminex
Light microscope	Primovert

Microcentrifuge	Roth
Mr.Frosty freezing container	Thermo Fisher
NanoDrop ™ 2000 / 2000c spectrophotometer	Thermo Fisher
LUNA™ Automated Cell Counter	Logos Biosystems
StepOne Plus Real-time PCR machine	Applied Biosystems
MP-220 PH-meter	Mettler Toledo
Pipettes	Eppendorf
PVDF membrane (Immobilon P, 0.45um)	Millipore
SDS-Page gel electrophoresis chamber	Bio-Rad
Semi-dry transfer system	Bio-Rad
Centrifuge 5415D Table top centrifuge	Eppendorf
Eppendorf Thermomixer comfort 1.5ml Thermal shaker	Eppendorf
Whatman paper(3MM)	Schleicher & Schuell
Wallac 1420 multilabel counter	Wallac Oy
Mini-PROTEAN® Tetra handcast systems	Bio-Rad
Keyence BZ-9000E	Keyence
Cytospin centrifuge Rotina 35R	Hettich

3.1.3 Commercial Kits

Kit name	**Manufacturer**
Direct-zol™ RNA MiniPrep	Zymo Research
SuperScript II reverse transcriptase 200U/µl	Invitrogen
Immobilon ECL ultra western HRP substrate	Millipore
Guava viacount reagents	Millipore
Molecular probes ImaGene green C12FDG lacZ gene expression kit	Thermo Fisher

Ghost Dye 780	Tonbo Bioscience
RIPA lysis buffer	Santa Cruz Biotechnology
4–15% Mini-PROTEAN® TGX™ Precast Protein Gels, 12-well	Bio-Rad
Precision Plus Protein ™ Dual Color Standards	Bio-Rad
Novex ™ NuPAGE ™ Sample Reducer (10X)	Invitrogen
Novex ™ NuPAGE ™ LDS Sample Buffer (4X)	Invitrogen
Lysosensor ™ green DND-189	Invitrogen
Pierce™ BCA Protein Assay Kit	Thermo Fisher

3.1.4 Antibodies

Name	**Manufacturer**
Rituximab	Roche
Obinutuzumab	Roche
β-Actin (8H10D10) Mouse mAb #3700	Cell signaling
Cleaved Caspase-3 (Asp175) (5A1E) Rabbit mAb #9664	Cell signaling
LAMP1 (D4O1S) Mouse mAb #15665	Cell signaling
Human p16 antibody (F-12) # sc-1661	Santa Cruz Biotechnology
Human Cathepsin B Antibody # sc-365558	Santa Cruz Biotechnology
Anti-Histone H3 (tri methyl K9) antibody #ab8898	Abcam
Anti-gamma H2A.X (phospho S139) antibody #ab11174	Abcam
Anti-Rabbit secondary antibody #NA934V	Cytiva
Anti-Mouse secondary antibody # NXA931	Cytiva

3.1.5 Cell lines in two subgroups

Cell line	**Manufacturer**	Subgroup
VAL	DMSZ	t+
DB	DMSZ	t+
DOHH2	DMSZ	t+
KARPAS422	ECACC	t+
NuDHL1	DMSZ	t+
OCILY1	DMSZ	t+
WSUDLCL2	DMSZ	t+
OCILY18	DMSZ	t+
SUDHL4	DMSZ	t+
SUDHL6	DMSZ	t+
SUDHL10	DMSZ	t+
Toledo	ATCC	t+
U2932	DMSZ	t-
OCILY7	DMSZ	t-
RCK8	DMSZ	t-
RI1	DMSZ	t-
SUDHL2	ATCC	t-
SUDHL5	DMSZ	t-

3.1.6 Media

RPMI complete medium	**Conc.**
FBS	10% v/v
Penicillin/ Streptomycin	100 U/mL

RPMI 1640

RPMI complete medium+ L-glutamine	Conc.
L-glutamine	10 mM
FBS	10% v/v
Penicillin/ Streptomycin	100 U/mL
RPMI 1640	

IMDM complete medium	Conc.
FBS	10% v/v
Penicillin/ Streptomycin	100 U/mL
IMDM	

Freezing medium	Conc.
Complete medium + FBS	1:1
DMSO	10%

3.1.7 Buffers and Solutions

Name	Composition
10% APS	1g Ammonium peroxysulfate in 10ml dH2 O
10% SDS (w/v)	10 g SDS in 100ml dH_2O
1.5M Tris-HCl (pH 8.8)	181.65 g Tris in 800ml dH_2O, adjust PH to 8.8
0.5M Tris-HCl (pH 6.8)	6 g Tris in 60ml dH_2O, adjust PH to 6.8
10x Tris-glycine Buffer	30.3g Tris

	144g Glycine in 1L dH_2O
1x SDS Running buffer (pH 8.3)	100ml 10x Tris-glycine Buffer 10ml 10% SDS (w/v) 890ml dH_2O
10x TBST	100ml 1.0M Tris-HCl (pH 8.0) 87.7g NaCl 5ml Tween-20 in 1L dH_2O
1.0M Tris-HCl (pH 8.0)	121.14 g Tris in 800ml dH_2O, adjust PH to 8.0
Anode Buffer I pH 10.4	18.5g Tris 50ml Methanol in 500ml dH_2O, adjust pH to 10.4
Anode Buffer II pH 10.4	1.51g Tris 50ml Methanol in 500ml dH_2O, adjust pH to 10.4
Cathode Buffer pH 9.4	1.51g Tris 1.44g Glycerin in 500ml dH_2O, adjust pH to 9.4
Blocking Buffer	2.5% BSA in 1x TBST
SA-β-gal fixation solution	0.25% Glutaraldehyde 2% Paraformaldehyde in PBS, prepare freshly
20xPotassium cyanide(KC) solution	20mg K3Fe(CN)6 1.05mg K4Fe(CN)6 x 3H2O in 25ml 1XPBS
SA-β-gal staining solution	9.3ml PBS 1mM Mgcl2(PH 6.0)

	0.5ml 20X KC solution
	0.25ml 40X X-Gal solution (40mg X-Gal in 1ml DMSO), prepare freshly
10% resolving gel (10ml)	3.3ml 30% Acrylamide/bis
	2.5 ml 1.5 M Tris-HCl, pH 8.8
	100 µl 10% SDS
	4.05ml distilled deionized water
	5 µl TEMED
	50 µl 10% APS
4% stacking gel (10ml)	1.32ml 30% Acrylamide/bis
	2.52 ml 0.5 M Tris-HCl, pH 6.8
	100 µl 10% SDS
	6ml distilled deionized water
	10 µl TEMED
	50 µl 10% APS
Stripping buffer	100mM glycine pH2.0

3.2 Methods

3.2.1 Cell culture

DLBCL cell lines were cultured in three complete mediums. VAL, DB, DOHH2, NUDHL1, OCILY18, RCK8, RI1, SUDHL2, SUDHL4, SUDHL6, SUDHL5, SUDHL10, Toledo, U2932, and WSUDLCL2 were in RPMI complete medium. KARPAS422 was in RPMI complete medium + L-glutamine. OCILY1, OCILY7 were in IMDM complete medium. A middle size flask with a filter cap was used. Cells might have grown as single cells or in small clusters. The subculture was performed by a dilution of 1:5 in fresh medium without centrifuge in 2-3 days. Cells were always kept growing in non-acidic conditions.

3.2.2 Cell counting method

The LUNA™ Automated Cell Counter was used with trypan blue staining. The dead cells were fully filled with trypan blue so that this would be a solid dot in the machine, while the living cell would be shown as a circle. The machine automatically calculated the viability and showed it on the screen. Cells were collected in a Falcon tube and centrifuged. With supernatant discarded and cells resuspended in fresh complete medium, the cell suspensions were mixed (1:1 v/v) with trypan blue. Next, 10 µl cell/trypan blue mixture was transferred to LUNA counting slide. The slide was then put into the machine and measured with the correct protocol.

3.2.3 Flow cytometry

Flow cytometry utilizes laser light to quantify cells and detect cell profiles in a heterogeneous fluid mixture. It has developed to be a popular analytical cell biology technology nowadays. Guava easyCyte™ 12HT Systems have 3 lasers and 14 parameters. The high-throughput option allows for a walkaway acquisition of up to 96 samples. A sample of fluorescently labeled cells is aspirated into the microcapillary flow cell. Forward and side scatter characteristics are detected by photodiodes. Fluorescence emission resulting from the excitation of fluorophores by the laser is

spectrally filtered and detected by several photomultiplier tubes (PMTs). The system can resolve the fluorescence from up to 12 fluorophores simultaneously.

3.2.3.1 Guava ViaCount assay

Guava ViaCount assay distinguishes between viable and non-viable cells based on the differential permeability of DNA-binding dyes in the Guava ViaCount Reagent. The nuclear dye stains only in the nucleated cells, thus excluding debris. The viability dye stains brightly in dead cells. The viable cells are finally stained as nuclear positive and dead cell negative. The fluorescence of each dye is resolved operationally to allow the quantitative assessment of both viable and non-viable cells present in a suspension. The debris is excluded efficiently. The assay is especially suitable for evaluating the efficacy of drugs after treatment.

3.2.3.1 C12FDG β-galactosidase activity assay

Fluorescein di-β-D-galactopyranoside (FDG) has been used for a highly sensitive flow cytometric β-galactosidase assay. 12-carbon fluorescein di-β-D-galactopyranoside (C12FDG) is a variant of FDG which has been covalently modified to include a 12-carbon lipophilic moiety. It has the important feature that it is permeable for living cells. It can be simply added in the medium of growing cells at ambient temperatures or at 37 °C. Once it goes inside the cell, the substrate is cleaved by β-galactosidase, producing a fluorescent product that is retained inside the cell. The product might have the incorporation of its lipophilic tail within the cellular membranes. C12FDG has the 497/518 excitation/emission spectrum. In Guava 12HT, it can be detected in the Green-B channel using the Incyte protocol.

3.2.4 Ab-mediated direct killing assay with Rituximab/Obinutuzumab for 24 hours

In the t+ group, the 12 cell lines DB, DOHH2, NUDHL1, OCILY1, OCILY18, KARPAS422, SUDHL4, SUDHL6, WSUDLCL2, VAL, SUDHL10, and Toledo were used. In the t- group, the 6 cell lines OCILY7, RCK8, RI1, SUDHL2, SUDHL5, and U2932 were used. For the 24h

cytotoxicity assay with Rituximab/Obinutuzumab, cells were collected by centrifuge in the Falcon tube, and then resuspended and counted using the LUNA cell counter. $3X10^5$ cells were calculated and seeded in the plate with a Rituximab or Obinutuzumab final concentration of 0, 0.1, 1, and 10 μg/ml. After 24 hours treatment, viable cells were measured with the Guava ViaCount assay protocol. Cells were collected and washed with 10ml PBS twice for excluding mAb. Guava ViaCount reagent was added for staining for 15-20 minutes. Cells were washed again with 10ml PBS. Trypsin was added for digesting mAb and aggregation for 5-10 minutes and measured by ViaCount protocol. This protocol is typically for obtaining single cell suspension after antibody treatment induced aggregation.

3.2.5 Senescence induction by ADR

Cells were collected by centrifuge in the Falcon tube, then resuspended and counted using the LUNA cell counter, and around 1.0×10^5 - 1.5×10^5 cells/ml were seeded in the plate. The final concentration of ADR in the DB, SUDHL2, SUDHL10, WSUDLCL2, KARPAS422, RI1, RCK8 cell lines was 10ng/ml, and in SUDHL6, SUDHL5, SUDHL4, OCILY1, OCILY7, and U2932 cell lines it was 5 ng/ml. Cells were treated with ADR for 3 days. The fresh medium was changed on day 3 without ADR. On day 5, cells were collected and stained with a solution including X-gal, following the SA-β-gal activity detection protocol.

3.2.6 SA-β-gal activity detection

The activity of SA-β-gal is the biomarker used for identifying the senescent phenotype. It is performed by histochemical staining the cells at pH 6.0 with the artificial substrate X-gal(5-bromo-4-chloro-3-indolyl-β-D-galactopyranoside). In the acidic environment, X-gal is quantitatively cleaved by the intracellular galactosidase depending on its activity and incubation time. A blue-dyed precipitate product which is water insoluble is generated by further oxidative cleavage.

After ADR treatment on day 5, cells were collected and washed by PBS. Around 15,000 cells were put into the slots of the cytospin instrument and centrifuged for 15 minutes. Freshly prepared 2% paraformaldehyde (PFA) plus 0.25% glutaraldehyde solution was used for fixation for 15 minutes at room temperature. Keeping the cells from drying is vital. The cells were washed twice with PBS

pH 6.0, to which 1mM MgCl2 was added. Freshly prepared SA-β-gal staining was put on top of the cells for staining at 37 °C in an incubator without CO_2. The staining intensity of untreated and treated cells was examined under the microscopy every few hours to get an optimal staining result. The staining conditions were kept constant for the same cell line. Photos were taken under the microscope with a 40X magnification in different areas in a bright field. ImageJ software was used for quantitatively counting the positive proportion of the samples.

3.2.7 Senolytic assay by detecting C12FDG

With induced into senescent status by ADR on day 5, the cells were collected by centrifuge in the Falcon tube, and then resuspended with pre-warmed fresh medium containing 33 μM C12FDG for 1 hour in an incubator at 37 °C. After washing once with medium without C12FDG, the cells were resuspended and counted using the LUNA cell counter, and $3x10^5$ viable cells were seeded with or without Rituximab or Obinutuzumab at a final concentration of 1μg/ml in the plate. After 24h, cells were collected for staining for flow cytometry measurement or for western blot. For flow cytometry measurement, cells were collected and washed with 10ml PBS twice to exclude mAb. Ghost dye 780/PI and permeable DNA binding dye blue (dilution 1:1000) were added for staining for 20 minutes. Ghost dye 780/PI was used to exclude dead cells. Permeable DNA binding dye was used to exclude debris. Cells were washed again with 10ml PBS. Trypsin was added for digesting mAb and aggregation for 5-10 minutes, and then measured by guava Incyte protocol. This protocol is typically for obtaining single cell suspension after antibody treatment induced aggregation.

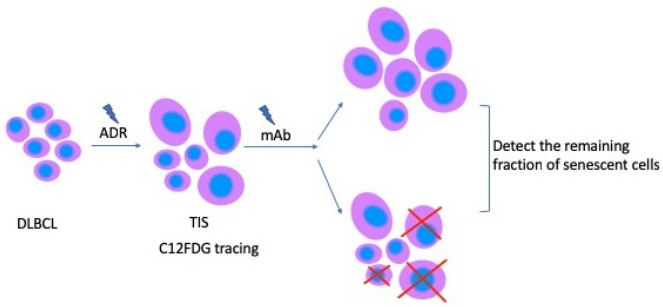

Figure 2. Schematic diagram of C12FDG tracing ADR-induced TIS followed by mAb treatment.

3.2.8 Western blot

3.2.8.1 Protein isolation

Protein pellets were collected as described in 3.2.7 and stored at -80 °C. The pallets were thawed on ice and lysed in RPIA buffer in which protease and phosphatase inhibitor had been included for 30 minutes. After centrifugation at 13,200 rpm for 20 minutes at 4°C, the supernatant containing proteins were transferred to a new Eppendorf vessel.

3.2.8.2 Protein concentration measurement (BCA method)

Bicinchoninic acid (BCA) assay is a method for colorimetrically detecting and quantifying the total protein in the sample. It combines the well-known reduction of Cu^{+2} to Cu^{+1} by protein in an alkaline medium (the biuret reaction) with the highly sensitive and selective colorimetric detection of the cuprous cation (Cu^{+1}) using a unique reagent containing bicinchoninic acid. The purple colored production of the assay is generated by the chelation of two molecules of BCA with one cuprous ion. The complex has a strongly absorbed light at a wavelength of 562nm. The amount of protein in the sample can be quantified by measuring the absorption spectra and comparing it with protein of an already known concentration. The Pierce™ BCA Protein Assay Kit was used. A range of diluted BSA standards (0, 25, 125, 250, 500, 750, 1000, 1500, and 2000 µg/mL) were prepared using RIPA buffer as the instruction's indicated. The experimental samples were diluted by 1:20 and seeded in duplicate in 96 wells. 200µl of reagent was added in each well including standards. The plate was mixed gently and put into the incubator at 37°C for 30 minutes. It was measured in the Wallac 1420 multilabel counter at a wavelength of 562nm. The concentration of experimental samples was calculated based on the standard curve in the Excel program.

3.2.8.3 Casting the gel

Use the Bio-Rad Mini-PROTEAN® Tetra handcast system. Assemble glass plates and spacers in the gel casting apparatus. Mix the components for the 10% resolving gel. Add APS and TEMED to the degassed acrylamide solution. Gently pour the mixture into the gel plates to a level 2 cm below the top of the shorter plate. Pace a layer of isopropanol on top. Allow the resolving gel to

polymerize for 30 minutes at room temperature. Drain the isopropanol and rinse with H_2O, then dry with filter paper. Mix the 4% stacking gel and pour it on top of running gel and insert the comb. Allow the gel to polymerize for at least 1 hour at room temperature or overnight at 4°C

3.2.8.4 Preparing Samples

22 µg protein in 25 µl volume including NuPAGE ™ Sample Reducer (dilution 1:10) and NuPAGE ™ LDS Sample Buffer (dilution 1:4) is boiled at 98°C for 5 minutes.

3.2.8.5 Running the gel

Remove the comb and assemble the casted gel into the Mini-Protean II apparatus. Add freshly prepared 1x running buffer and load the boiled samples into the wells of the gel. Run the gel at 100 V until the dye front migrates into the running gel, and increase this to 150 V until the dye front reaches the bottom of the gel.

3.2.8.6 Semi-dry transfer

Prepare the anode and cathode buffer, PVDF membrane, and a 3MM Whatman filter paper sized the same as the gel. Remove the gel from the cassette, then trim away the stacking gel. Immerse the gel in cathode buffer for 5-10 minutes. Soak one piece of 3MM paper in anode buffer Ⅰ, two pieces of 3MM paper in anode buffer Ⅱ, and three pieces of 3MM paper in cathode buffer for at least 30 seconds. Wet the membrane in methanol for 15 seconds and place it in anode buffer Ⅱ for equilibration for at least 5 minutes. Place the anode electrode plate on a level benchtop. Place one piece of paper soaked in anode buffer Ⅰ in the center of the plate. Place two papers soaked in anode buffer Ⅱ on top of the first sheet. Place the membrane on top of the papers. Place the gel on top of the membrane. Place three papers soaked in cathode buffer on top of the membrane. Ensure that there is no bubble between every layer. Place the cathode electrode plate on top of the stack. Run the Semi-dry transfer machine (Bio-Rad) at 25V for 45 minutes.

3.2.8.7 Immunoblotting

Block the membrane with 2.5% BSA in TBST for 30 minutes at room temperature on the shaker. Prepare the primary antibody in 5% BSA TBST solution (dilution 1:1000) and cover the membrane on the shaker for 2 hours at room temperature or overnight at 4°C. Wash the membrane for 10 minutes 3 times in TBST. Pour off the secondary antibody diluted at 1:20,000 in TBST solution for 30 minutes on the shaker at room temperature. Wash again for 10 minutes 3 times with TBST solution. Make images with the FUJIFILM LAS4000. Prepare the ECL substrate at 1:1. Incubate the membrane in the substrate for 5 minutes. Expose the membrane in the machine for imaging. Use ImageJ as the quantification software. Normalize data by loading control β-Actin and ADR mAb double untreated samples.

3.2.9 Lysosensor green detection assay

Lysosensor green probes are pH indicators that can partition into acidic organelles in the living cell. These give a way for researchers to study the dynamic aspect of lysosome biogenesis and function. The dye is acidotropic and accumulates in acidic organelles like lysosomes as a result of protonation. The protonation can relieve the fluorescence quenching of the dye by its weak base side chain, resulting in an increase in fluorescence intensity. In different conditions, the dye becomes more fluorescent in acidic environments. The acid dissociation constant pK_a of the Lysosensor green DND-189 is ~ 5.2.

With induced into senescent status by ADR on day 4, the cells were collected by centrifuge in the Falcon tube, then resuspended with pre-warmed fresh medium containing Lysosensor green (dilution 1:1000) overnight in an incubator at 37 °C. On day 5, cells were collected and seeded with fresh medium containing Lysosensor green and Rituximab/Obinutuzumab and PI (dilution 1:2000). Images were made using the time-relapse mode in the Keyence machine. The software ImageJ was used to do the quantification of the images.

3.2.10 Quantitative Real-Time PCR

Based on the principle of the conventional polymerase chain reaction (PCR), quantitative PCR is a method to quantify the DNA product at the end of the reaction. By means of fluorescence, the product can also be recorded during a PCR cycle in real time. The fluorescence increases

proportionally with the accumulation of the PCR product. Correct quantification is only possible in the exponential phase of PCR. The Applied Biosystem Taqman assay is one of the quantitative real-time PCR systems. It consists of a pair of unlabeled PCR primers and a Taqman probe with a dye label (FAM) on the 5' end and a minor groove binder (MGB) and non-fluorescent quencher (NFQ) on the 3' end.

3.2.10.1 RNA isolation

Add an appropriate volume (500µl-700µl) of Trizol reagent to the cell pellet and mix thoroughly. Centrifuge and transfer the supernatant to an RNase-free tube. Add an equal volume of ethanol to the sample. Transfer the mixture into a Zymo-Spin IIC Column into a collection tube and centrifuge. Add DNase I to the column matrix and incubate for 30 minutes. Add 400 µl Direct-zol RNA PreWash to the column and centrifuge. Add 700 µl RNA Wash Buffer to the column and centrifuge. Add 30 µl DNase/RNase-Free Water to the column and centrifuge. Measure the concentration using a NanoDrop ™ 2000 / 2000c spectrophotometer. Store the RNA at -80°C.

3.2.10.2 SuperScript II Reverse Transcription

Mixture 1	**Volume**
Oligo(dT) $_{12\text{-}18}$(500 µg/mL)	1µL
dNTP Mix (10 mM each)	1µL
RNA + dH_2O	11 µL
Total	13 µL

Table 6. Reverse transcription mixture 1 components.

Mixture 2	**Volume**
5X First-Strand Buffer	4µL
0.1 M DTT	2µL
RNaseOUT ™ (40 units/µL)	0.5µL
SuperScript ™II RT	0.5 µL

Table 7. Reverse transcription mixture 2 components.

1 µg RNA was used for the reverse transcription. Mixture 1 was heated at 65°C for 5 minutes to 4°C. Add 7µL of mixture 2 and incubate at 42°C for 50 minutes, followed by heating at 70°C for 15 minutes. Store the cDNA at -20°C.

3.2.10.3 qPCR

10 µL reaction mixture	**Volume**
Taqman master mix	5µL
Taqman primers	0.5µL
cDNA	3µL
dH_2O	1.5 µL

Table 8. qPCR mixture components.

Cycles	**Temperature**	**Time**
1	95°C	2 min
40	95°C 60°C	5 sec 20 sec

Table 9. qPCR cycling conditions.

RPL19 was used as an internal control transcript which was not expected to change during the experimental interventions. The relative expression level of the gene was calculated using the following parameters: $2^{(-\Delta\Delta Ct)}$ which $\Delta\Delta Ct = \Delta Ct_{treated} - \Delta Ct_{untreated}$.

3.2.11 Statistical analysis

Data are expressed as mean ± SD, n stands for the number of independent cell lines. GraphPad Prism software was used for the statistical analysis. The data was first explored to check normal distribution with the Shapiro–Wilk test and Kolmogorov-Smirnov goodness-of-fit test and histogram. The paired t-test was used with normal distribution, otherwise the Wilcoxon matched-pairs signed rank test was used. The Mann-Whitney test was used for qRT-PCR data and other unpaired data. Differences were considered significant when the *p*-value was smaller than 0.05. The following symbols were used: * for $p < 0.05$, ** for $p < 0.01$.

4 Results

4.1 Ab-mediated direct killing of Obinutuzumab

Ab-mediated direct killing is one of the main functions of antibodies besides ADCC, ADCP and CDC. Because of the very high heterogeneity in DLBCLs, a total of 18 cell lines in the two subgroups - 12 t+ and 6 t- - were used to evaluate the Ab-mediated direct killing of Rituximab and Obinutuzumab. There are less cell lines in the t- group due to it being harder to establish them in ABC DLBCL cell lines, which would depend more on an environment of BCR ligands not present in the culture. The binding force between epitope and paratope is decided by their specific molecular constitution and therefore, a different antibody would have different saturating concentration which confers the highest binding efficacy. To compare the capability of the two mAbs comprehensively, the experiment was designed with three different concentrations (0.1, 1, and 10 μg/ml) for 24 hours treatment in parallel. To get a more accurate result, the flow cytometry-based cell counting method was used for cells stained with Guava ViaCount reagent to exclude debris by staining living cells with DNA specific binding dye which is permeable for intact cell membrane. A common feature of cell population treated with mAb *in vitro* is aggregation that would compromise the measurement accuracy by flow cytometry by either blocking the capillary of the machine or increasing the false positive percentage of dead cells. To solve this problem, trypsin was used for a short time (5-10 minutes) at the final step before measurement to obtain a single cell suspension solution. Figure 3 is a summary of results of all cell lines treated with Rituximab or Obinutuzumab, normalized to the viable cell number of untreated samples. At 0.1 μg/ml concentration, Obinutuzumab is more effective than Rituximab in both the t+ subgroup ($p = 0.0058$) and in the t- subgroup ($p = 0.0141$). There is no difference between the t+ subgroup and the t- subgroup after Obinutuzumab treatment. At 1 μg/ml concentration, Obinutuzumab is more effective than Rituximab in both the t+ subgroup ($p = 0.0196$) and in the t- subgroup ($p = 0.0334$). There is no difference between the t+ subgroup and the t- subgroup after Obinutuzumab treatment. At 10 μg/ml concentration, Obinutuzumab is more effective than Rituximab in the t+ subgroup ($p = 0.0232$) and in the t- subgroup ($p = 0.0179$). At this concentration of 10 μg/ml – close to

concentrations typically used *in vitro* for anti-CD20 antibodies in direct cytotoxicity assays in the literature[17(p20),28] – Obinutuzumab has superiority in the t+ subgroup compared to in the t- subgroup (p = 0.0415), thereby reproducing a pivotal result unveiled by the post-protocol analysis of the GOYA trial in this – certainly highly simplified – cell-autonomous kill assay.[37]

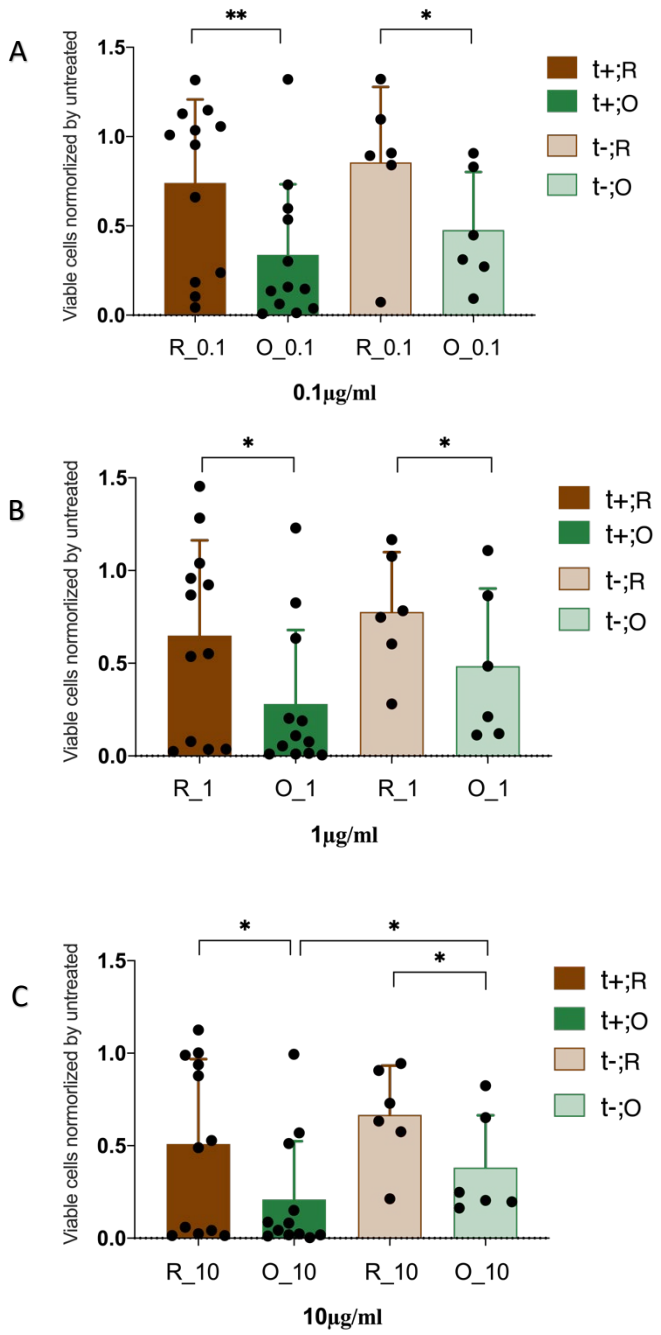

Figure 3. Ab-mediated direct killing of Obinutuzumab.

Viable cell numbers were measured by flow cytometry after 24h treatment with Rituximab (R) or Obinutuzumab (O) in three different concentrations (0.1, 1, 10 µg/ml) in 12 t+ and 6 t- cell lines. Data was normalized by untreated

sample. Each dot represents one cell line. The column and bar represent mean ± SD. * $p < 0.05$, ** $p < 0.01$. **(A)** Rituximab or Obinutuzumab treatment concentration was 0.1 μg/ml. **(B)** Rituximab or Obinutuzumab treatment concentration was 1 μg/ml. **(C)** Rituximab or Obinutuzumab treatment concentration was 10 μg/ml.

4.2 Obinutuzumab had higher senolytic capability in the t+ subgroup

4.2.1 ADR induced senescence in both subgroups

The standard treatment for DLBCL patients in clinic is the combination of chemotherapy and monoclonal antibody. In chemotherapy, CHOP includes three DNA- or spindle-damaging cytotoxic poisons (Cyclophosphamide, Vincristine, ADR), which may induce cellular senescence. To facilitate the chemo-like treatment of cell lines *in vitro*, a single agent was selected based on following reasons. Cyclophosphamide needs to be converted to active metabolites by oxidase enzymes in the liver. Phosphoramide mustard is the main effector form of cyclophosphamide, which could make DNA crosslinks at guanine N-7 positions, leading cells to apoptosis. Vincristine works by stopping the tubulin dimers from polymerizing to form microtubules through binding to the tubulin protein. Therefore, cells treated with vincristine would be unable to separate the chromosomes during the metaphase, and not at the G1 phase like in senescence. ADR (also known as Doxorubicin) interacts with DNA by intercalation and inhibition of macromolecular biosynthesis. It stabilizes the topoisomerase II complex after the DNA chain is broken, preventing the DNA double helix from being resealed to stop the process of replication. Hence, ADR was opted for as a key representative of these CHOP components, likely to entertain apoptosis and TIS in a very similar way to other DNA-damaging cytotoxic CHOP components in this project. All 18 cell lines were tested to induce to senescence. With different susceptibility to ADR, five cell lines including VAL, DOHH2, NUDHL1, OCILY18, and Toledo were failed because of less than 20% viability after 5ng/ml ADR treatment. 7 cell lines in the t+ subgroup and 6 cell lines in the t- subgroup were successfully induced to senescence. In DB, SUDHL10, WSUDLCL2, and KARPAS422 in the t+ subgroup and SUDHL2, RI1, and RCK8 in the t- subgroup, ADR concentration was 10ng/ml. In SUDHL6, SUDHL4, and OCILY1 in the t+ subgroup and SUDHL5, OCILY7, U2932 in the t- subgroup, ADR concentration was 5 ng/ml. Summarized data of the cell line numbers in two groups with two ADR concentrations is shown in Table 8. On day

five, cells were collected and evaluated for the SA-β-gal activity. Representative images of SA-β-gal staining are shown in Figure 4A for 7 t+ cell lines and in Figure 4B for 6 t- cell lines. After quantification (Figure 4C), both subgroups show high SA-β-gal activity after treatment (t+ subgroup, $p < 0.001$; t- subgroup, $p < 0.001$). In the t+ subgroup, there is higher SA-β-gal activity than in the t- subgroup ($p = 0.044$).

		ADR concentration	
		5 ng/ml	10 ng/ml
Groups	t+	4	3
	t-	3	3

Table 10. Cell line numbers in two groups with two ADR concentrations in senescence induction.

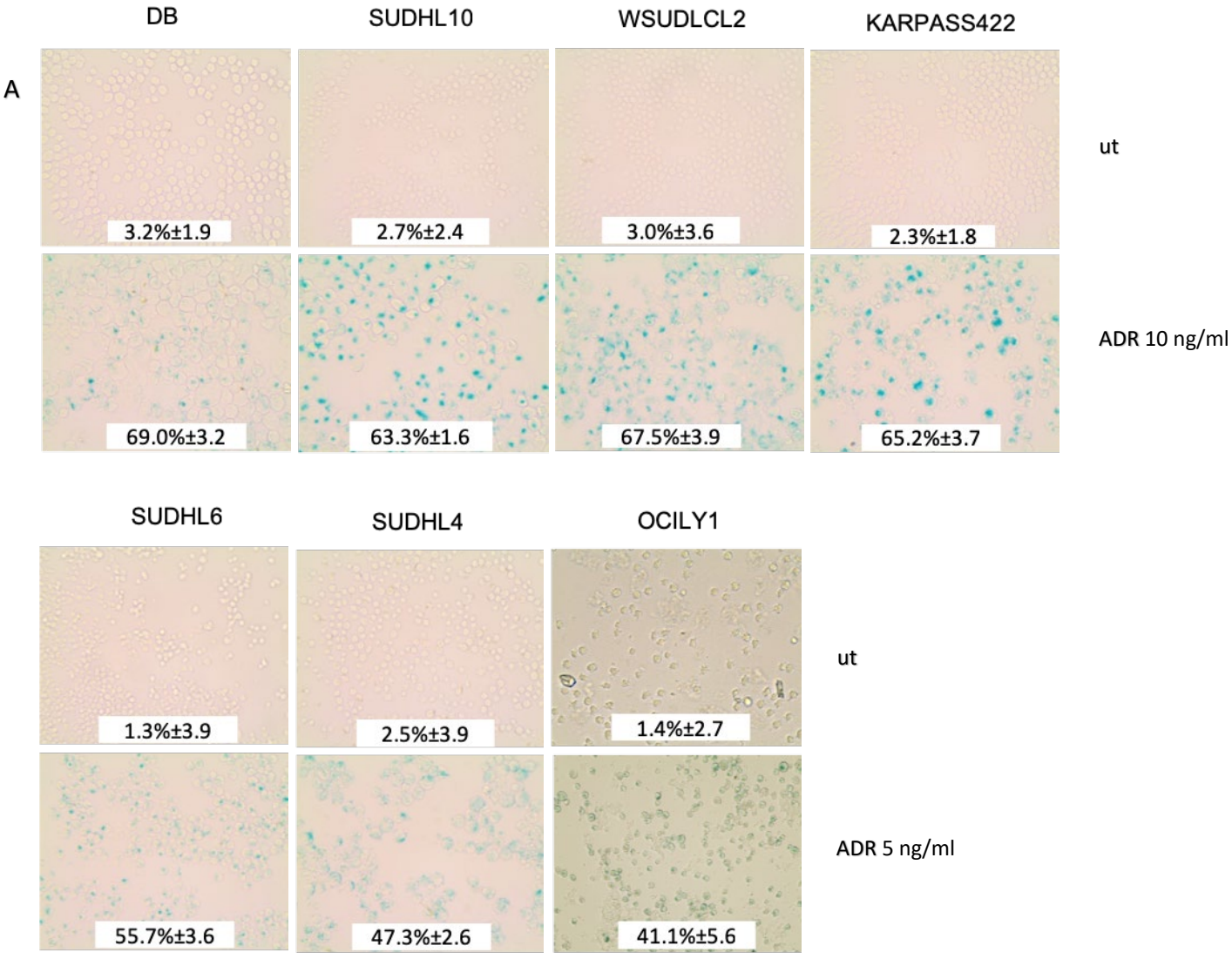

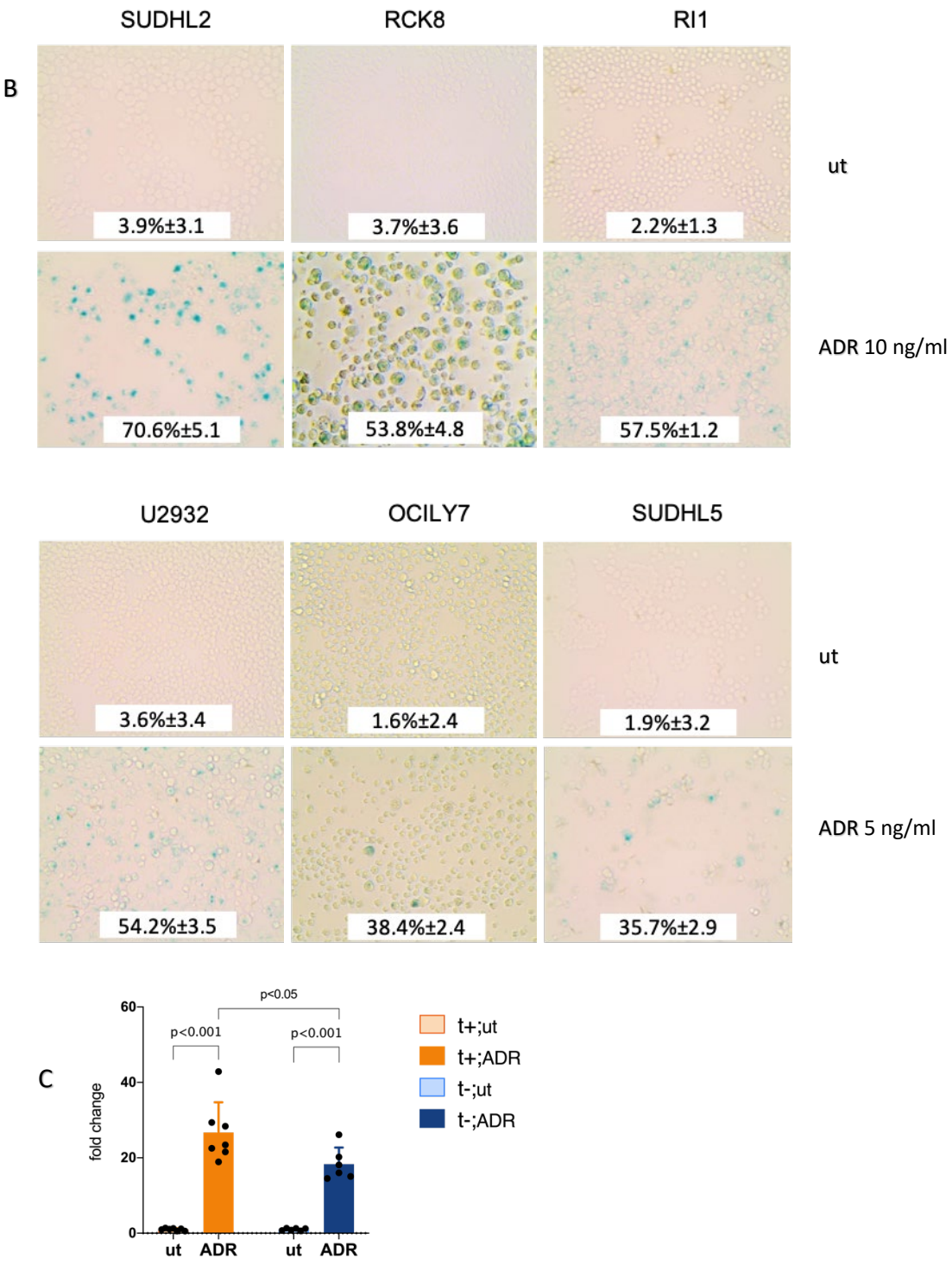

Figure 4. ADR induced senescence had high SA-β-gal activity in both subgroups.

Cells were treated with ADR for five days and evaluated for SA-β-gal activity. **(A)** SA-β-gal activity in the t+ subgroup, n = 7. **(B)** SA-β-gal activity in the t- subgroup, n = 6. **(C)** Comparison of SA-β-gal activity in the two subgroups. The column and bar represent mean ± SD.

4.2.2 Increased SASP and SAS gene expression in ADR-senescent cells

On day five after ADR treatment, cells were collected to extract RNA. The expression of SASP genes (CCL2, IL6, IL1α) and SAS genes (CD44, CD133) was measured by qPCR after cDNA was transcribed. In both subgroups, there was increased SASP and SAS gene expression. There was no difference between the two subgroups. This is another aspect that could confirm the senescence status by ADR treatment. Data are shown in Figure 5.

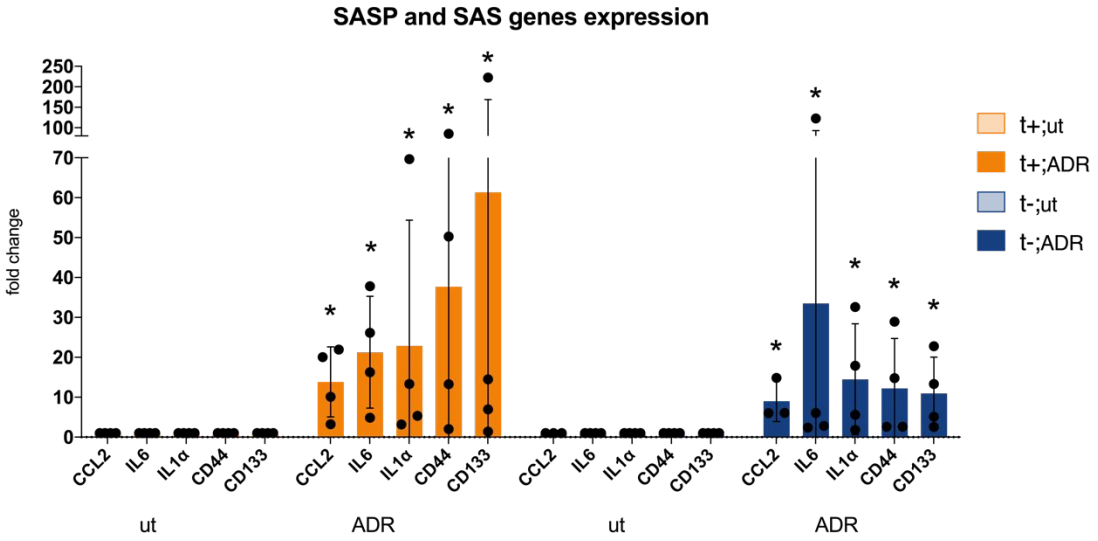

Figure 5. ADR induced senescence had increased SASP and SAS gene expression in both subgroups.

Relative expression of genes was calculated using ΔΔCt. Each dot represents one cell line. In both subgroups, n = 4. The column and bar represent mean ± SD. * $p < 0.05$.

4.2.3 CD20 expression was not changed after senescence induction by ADR in both subgroups

The amount of antibody that binds to a cell is decided by the amount of surface antigen. Until saturation is reached, a higher expression of antigen would confer higher antibody binding efficacy. To check if CD20 expression is changed after senescence, qRT-PCR was done for the samples before and after senescence. Figure 6 demonstrates that there is no difference in CD20 expression before and after senescence induction by ADR in both subgroups.

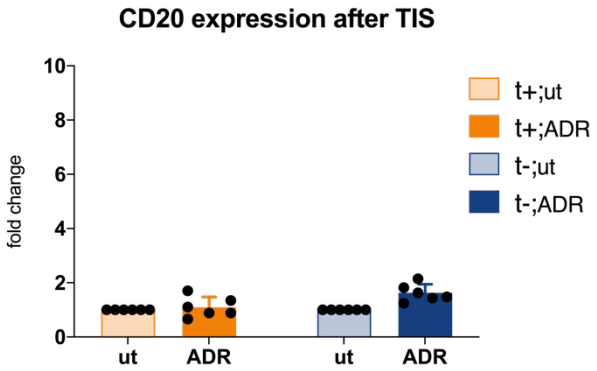

Figure 6. CD20 expression was not changed after senescence induction by ADR in both subgroups.

Relative expression of genes was calculated using ΔΔCt. Each square represents one cell line. In both subgroups, n = 6. The column and bar represent mean ± SD.

4.2.4 Obinutuzumab had higher senolytic capability in the t+ subgroup

The role of mAb in the combination of chemotherapy plus mAb treatment besides its individual function in DLBCL patients was elucidated by our work[28], in that rituximab could induce lymphoma cells to senescence and rituximab-based immunotherapy could sensitize lymphoma cells to ADR-induced senescence, depending on elevated ROS by exposing lymphoma cell lines in Rituximab with a cross-linker or in combination with ADR. Hence, by reversing the sequence from the other side, using the mAb secondarily after ADR treatment would have two aspect effects depending on the intensity of damage, senescence induction and killing enhancement. The proportion of senescent cells after secondary mAb treatment could reflect an underestimation, if mAb also induces lots of senescent cells, on the other hand, and operates as killing agent (including non-senescent cells killing and senolysis). The remaining fraction of senescent cells are biologically essential. Weak killing efficacy would be revealed if virtually all cells remained in senescent status, or the senolytic effect plays dominantly with a lot less senescent cells left. However, even having few senescent cells may become clinically relevant if they undergo reprogramming and gain stemness capacity. To trace the senescent cells, the fluorescent dye C12FDG was applied on day five after ADR treatment. The proportion of C12FDG-positive population was measured by flow cytometry. The senolytic effect of Rituximab and Obinutuzumab was measured by counting the number of viable C12FDG-positive cells after 24 hours of mAb treatment, reflecting the amount of the senescent cells that were killed by the mAb based on the

normalization with untreated samples. The green fluorescence of C12FDG is sensitive and the accurate quantification of it is feasible by flow cytometry. Dead cells and debris are easily excluded by staining with the relevant dye. 7 t+ cell lines and 6 t- cell lines were tested and the results are summarized in Figure 7. The intensity of C12FDG was significantly decreased by Obinutuzumab compared to Rituximab (ADR-O vs ADR-R, $p = 0.0047$), with virtually no such effect detectable for Rituximab (ADR-O vs ADR-ut, $p = 0.0042$) in the t+ subgroup (Figure 7A). In stark contrast, no such effect became detectable in the t- subgroup (Figure 7A). The corresponding living cell number was also decreased by Obinutuzumab compared to Rituximab (ADR-O vs ADR-R, $p = 0.039$), and compared to untreated samples (ADR-O vs ADR-ut, $p = 0.047$) in the t+ subgroup (Figure 7B). In the t- subgroup, the senescent cells were not killed (Figure 7B).

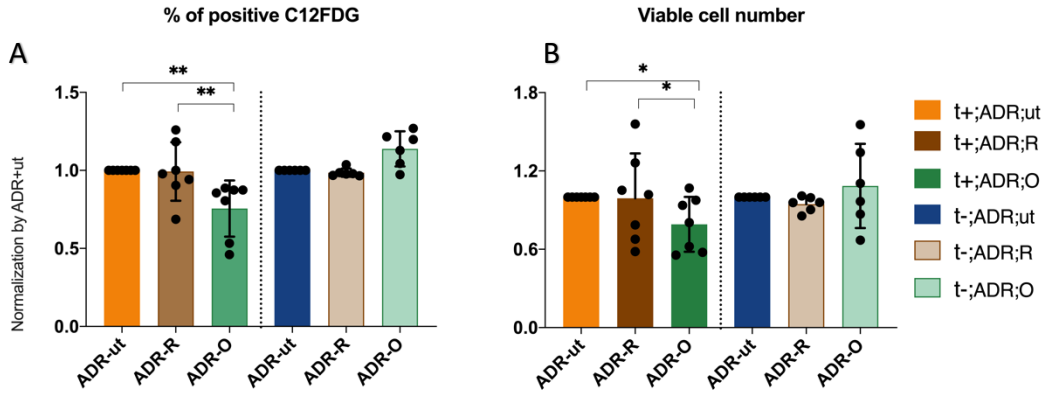

Figure 7. Obinutuzumab had higher senolytic capability in the t+ subgroup by C12FDG detection.

The intensity of C12FDG was measured after secondary treatment on ADR treated samples with Rituximab (ADR-R) or Obinuzumab (ADR-O) or untreated (ADR-ut) for 24h by flow cytometry. In the t+ subgroup n = 7. In the t- subgroup n = 6. The data is normalized by ADR-ut. Each dot represents one cell line. The column and bar represent mean ± SD. * $p < 0.05$. **(A)** percentage (%) of positive C12FDG. **(B)** corresponding viable cell number of A.

4.2.5 Senolysis confirmed by western blot

To make further confirmation of the senolytic effect of Obinutuzumab and Rituximab, protein extract was prepared from 6 t+ and 4 t- cell lines after the secondary treatment with mAb for 24 hours. Three senescence markers (phosphorylated form of H2A histone family (γH2AX), p16 and

Histone 3 lysine 9 trimethylation (H3K9me3)) were used for monitoring the senescence induced by ADR and senolysis induced by mAb. γH2AX is the phosphorylation of the Ser-139 residue of the histone variant H2AX. It exists as an early cellular response to DNA damage initiating therapy-induced senescence. With the accumulation of DDR, p16 is activated and H3K9me3 is formed and maintained during the senescence process. The induction of these three markers were tested by western blot. 6 t+ cell lines (Figure 8A) and 3 t- cell lines (Figure 8B) were included. The quantification of WB in both subgroups was summarized (Figure 8C, 8D, 8E). After 24h treatment with mAb, p16 and H3K9me3 expression were significantly decreased and the effect of Obinutuzumab was more than of Rituximab in the t+ subgroup (p16, ADR-O VS ADR-R, p = 0.0382; H3K9me3, ADR-O vs ADR-R, p = 0.0312). γH2AX also showed a similar trend. There was no difference between Obinutuzumab and Rituximab for these three markers in the t- group.

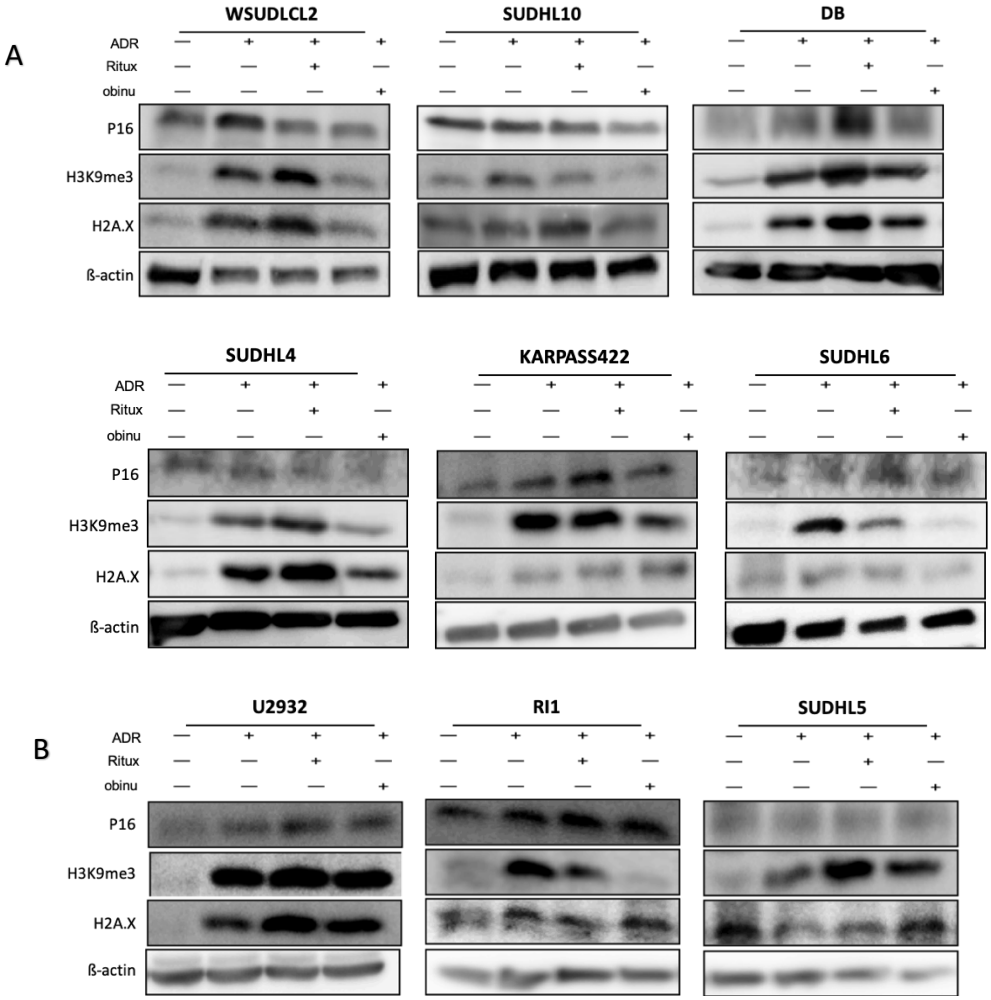

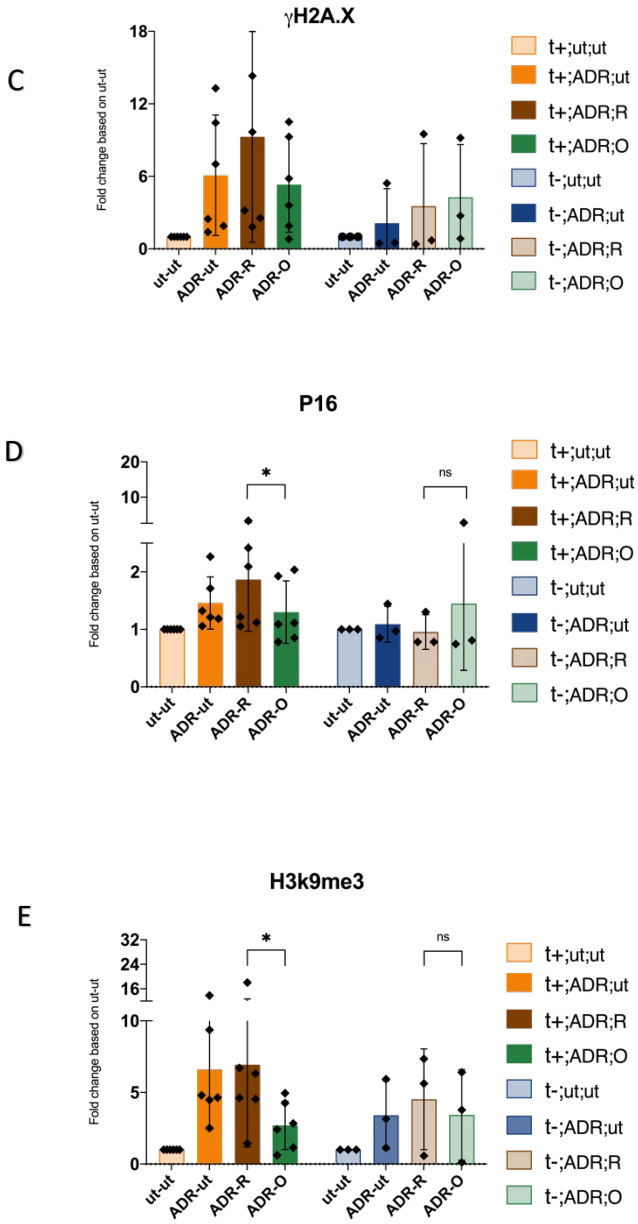

Figure 8. Senolysis confirmed by western blot.

The protein expression of γH2AX, p16, and H3K9me3 were measured after secondary treatment on ADR treated samples with Rituximab (ADR-R) or Obinuzumab (ADR-O) or untreated (ADR-ut) for 24h by WB. In the t+ subgroup n = 6. In the t- subgroup n = 4. **(A)** The protein expression of γH2AX, p16, and H3K9me3 in the t+ subgroup. **(B)** The protein expression of γH2AX, p16, and H3K9me3 in the t- subgroup. **(C)** Quantification of γH2AX expression in both subgroups. **(D)** Quantification of p16 expression in both subgroups. **(E)** Quantification of H3K9me3 expression in both subgroups. For quantification, the data was normalized by β-Actin and ADR mAb double untreated. Each rhombus represents one cell line. The column and bar represent mean ± SD. * $p < 0.05$.

4.2.6 Senolytic effect of Obinutuzumab in the t+ subgroup was associated with lysosomal function

It has been reported that Ab-mediated direct killing by Obinutuzumab is associated with lysosomal cell death. To further explore the senolytic effect of Obinutuzumab in the t+ subgroup, the apoptosis marker cleaved caspase-3 and lysosome status were checked by WB. Cleaved caspase-3 was picked because caspase-3 activation happens in both intrinsic and extrinsic induction of apoptosis. Results are shown in Figure 9. The multibands in Cathepsin B are mainly due to it being produced from a larger precursor form pro-cathepsin B and it is proteolytically processed and glycosylated to form mature protein, with a broad range of molecular weight (24~44 kDa). Apoptosis was induced during the senescence induction process by ADR in both subgroups, as shown by increased cleaved caspase-3 level. However, the level of cleaved caspase-3 did not increase after Obinutuzumab treatment in the t+ subgroup, indicating that apoptosis was not involved during Obinutuzumab-mediated senolysis. As another mechanism of cell death during senolysis, lysosomal cell death markers were checked. Lamp1 is the lysosome membrane protein and Cathepsin B is one of the most important hydrolysis enzymes inside the lysosome. Both Lamp1 and Cathepsin B expression were not changed much during senescence induction and senolytic processes. This result contradicted previous publications by many authors, therefore, I suspected technical problems in the experimental setting or sample preparation, and sought to monitor lysosmal function with a different method.

As an alternative way to monitor lysosomal function, Lysosensor green was applied to trace lysosome pH change during the process of senolysis by Obinutuzumab. Lysosomes have an acidic pH ~4.8 when compared to the slightly basic cytosol (pH 7.2). Lysosensor green is a fluorescent pH indicator and used for studying the dynamic aspect of lysosome biogenesis and function. Lower pH would give out a higher intensity of green fluorescence, indicating increased lysosomal activity. After senescence induction by ADR treatment, cells were stained with LysoSensor and PI (marking dead cells). Images were taken to trace the pH change of lysosomes after around 15 minutes and 2 hours of secondary treatment with mAb. Figure 9E is the result of one representative

cell line from each of the two subgroups. Decreased green fluorescence was observed after Obinutuzumab treatment in the t+ cell lines. More dead cells were seen as red dots after Obinutuzumab treatment in the t+ cell lines. This change was not observed in the t- subgroup. In total, 4 cell lines in the t+ subgroup and 3 cell lines in the t- subgroup were measured. Quantification of Lysosensor staining is shown in Figure 9F. The pH of lysosome in the t+ subgroup was increased after secondary treatment with Obinutuzumab, which was not observed in the t- subgroup. Figure 9G shows the quantification of PI staining of dead cells (shown in Figure 9E, red dots) in corresponding samples. There were more dead cells in the t+ subgroup by secondary treatment with Obinutuzumab. In essence, these data are consistent with a disruption of the acidic lysosomal compartment in ADR-senescent cells upon intervention with Obinutuzumab, but not with Rituximab, further supporting the concept that Rituximab rather enhances ADR-induced senescence, while Obinutuzumab selectively eliminates senescent cells, mirrored by a lack of biochemical features of senescence in the remaining, surviving cells.

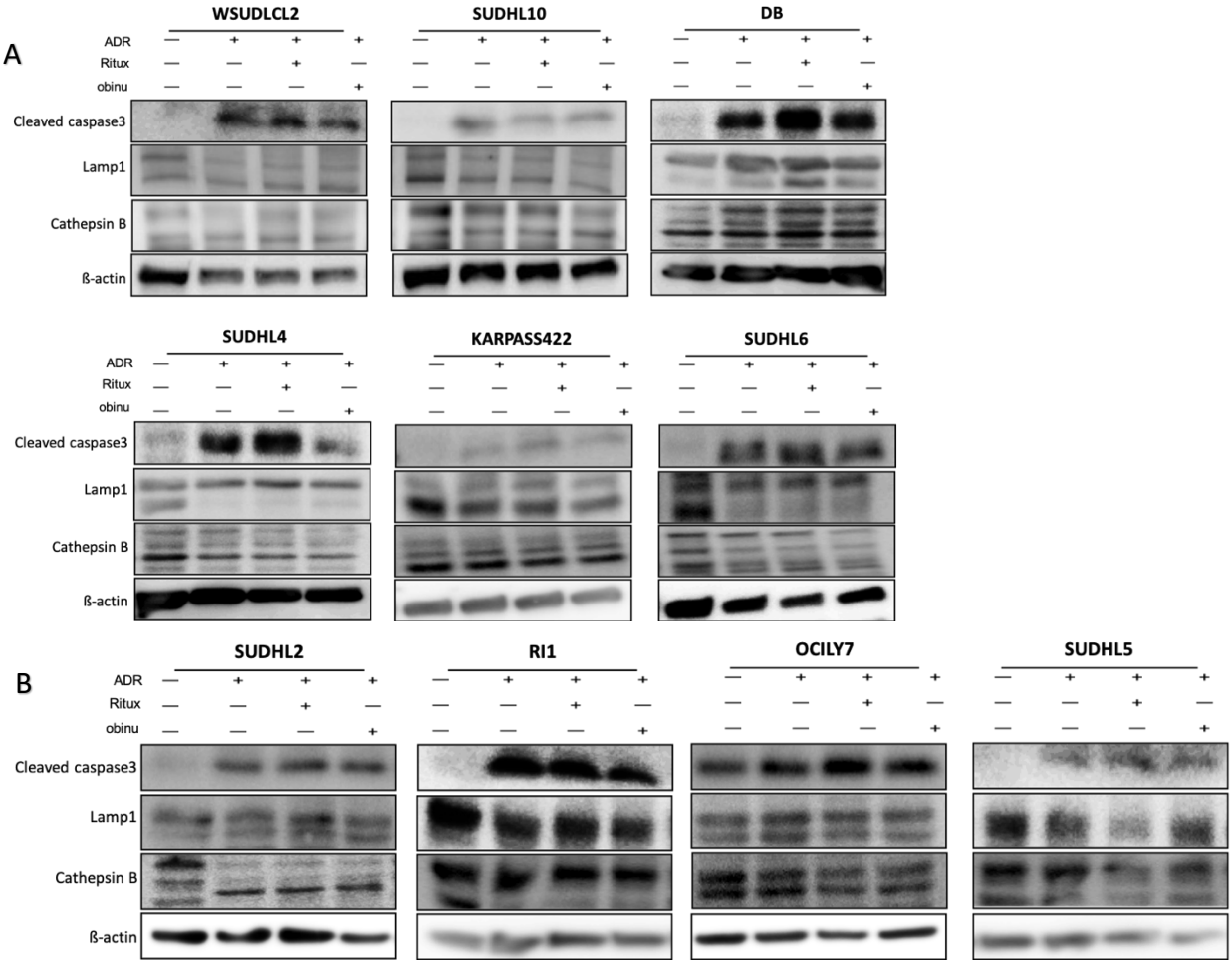

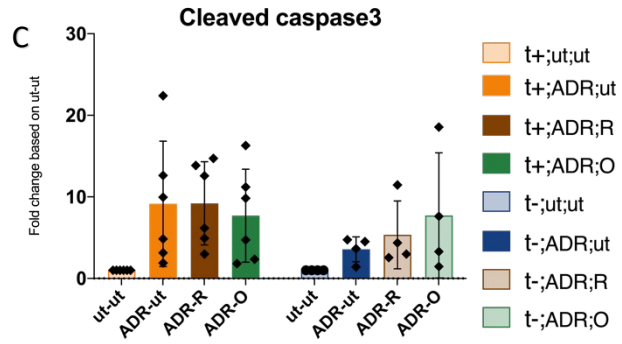
C
Cleaved caspase3
Fold change based on ut-ut
30
20
10
0
ut-ut
ADR-ut
ADR-R
ADR-O
t+;ut;ut
t+;ADR;ut
t+;ADR;R
t+;ADR;O
t-;ut;ut
t-;ADR;ut
t-;ADR;R
t-;ADR;O

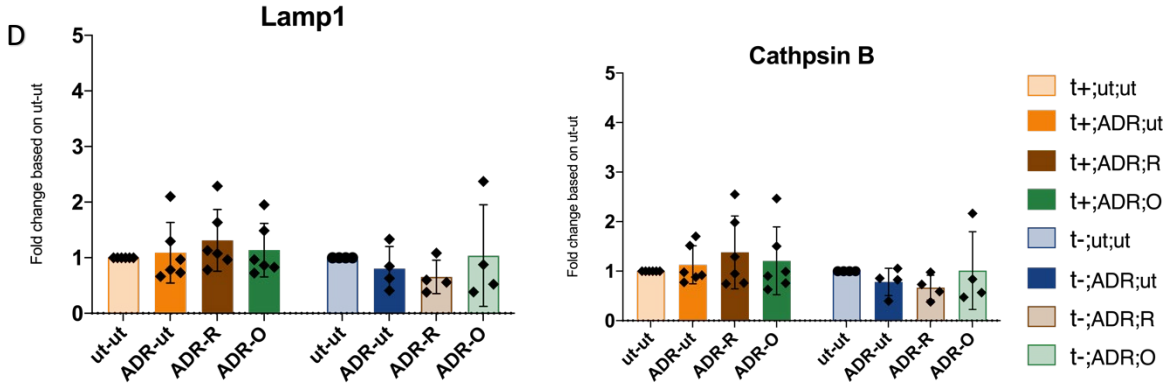
D
Lamp1
Fold change based on ut-ut
5
4
3
2
1
0
ut-ut
ADR-ut
ADR-R
ADR-O
Cathpsin B
t+;ut;ut
t+;ADR;ut
t+;ADR;R
t+;ADR;O
t-;ut;ut
t-;ADR;ut
t-;ADR;R
t-;ADR;O

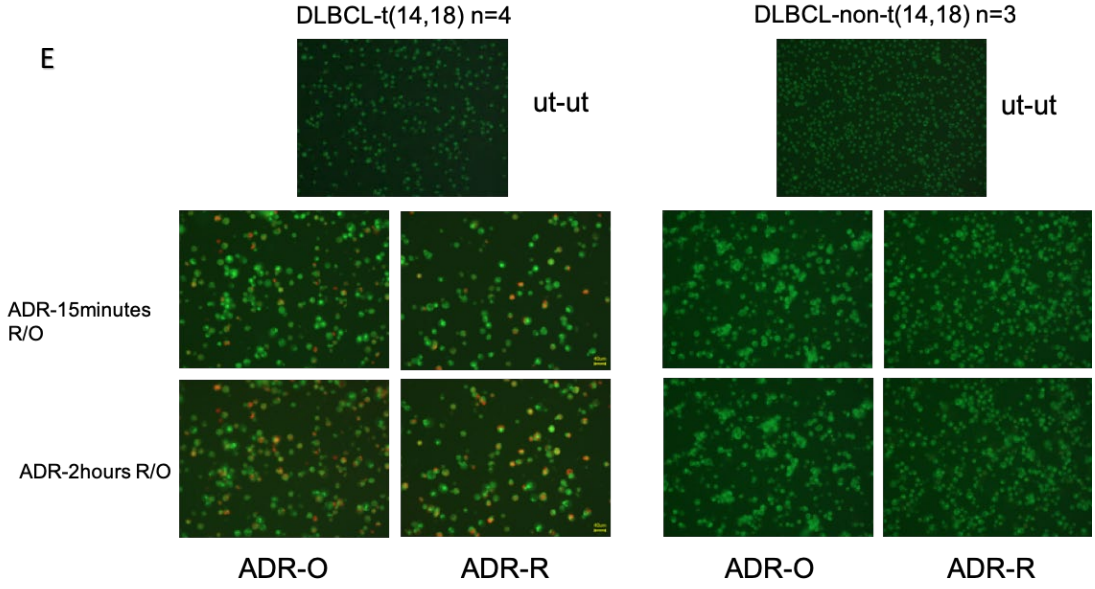
E
DLBCL-t(14,18) n=4
DLBCL-non-t(14,18) n=3
ut-ut
ut-ut
ADR-15minutes
R/O
ADR-2hours R/O
ADR-O
ADR-R
ADR-O
ADR-R

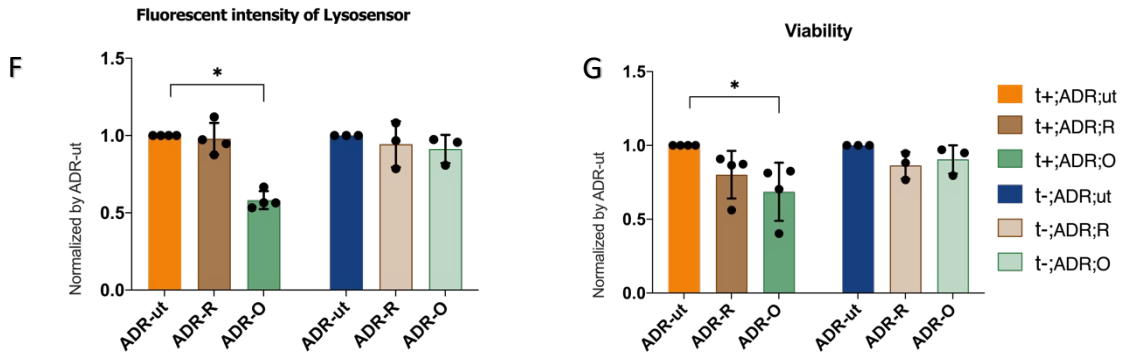

Figure 9. Senolytic effect of Obinutuzumab in the t+ subgroup was associated with lysosomal function.

The protein expression of cleaved caspase3, lamp1, and cathepsin B was measured after secondary treatment on ADR treated samples with Rituximab (ADR-R) or Obinuzumab (ADR-O) or untreated (ADR-ut) for 24h by WB. In the t+ subgroup n = 6. In the t- subgroup n = 4. **(A)** The protein expression of cleaved caspase3, lamp1, and cathepsin B in the t+ subgroup. **(B)** The protein expression of cleaved caspase3, lamp1, and cathepsin B in the t- subgroup. **(C), (D)** Quantification of cleaved caspase3, lamp1 and cathepsin B expression in both subgroups. For quantification, the data was normalized by β-Actin and ADR mAb double untreated. Each rhombus represents one cell line. The column and bar represent mean ± SD. **(E)** Images of one representative cell line from each subgroup to show PH change; red dots are dead cells stained with PI. **(F)** Quantification of PH change in 4 t+ and 3 t- cell lines. **(G)** Quantification of viability in the corresponding cell lines in (F).

5 Discussion

Efforts were made toward the manipulation of type II anti-CD20 antibody to generate Obinutuzumab which was done with advanced therapeutic antibody engineering technology, like removing fucose on the Fc region. Unfortunately, the GOYA trial demonstrated no significant difference between O-CHOP and R-CHOP for both the OS and PFS of DLBCL patients. However, when applied with the LPS platform and only strong GCB patients were taken, O-CHOP showed higher superiority in the PFS rate than R-CHOP and the same result was achieved with the GALLIUM trial for FL patients. Interestingly, when the GOYA trial was checked by fluorescence in situ hybridization (FISH), for translocation between chromosome 14 and 18, a characteristic genomic change of FL, strong GCBs were more prone to this reminiscent characteristic. This translocation incidence rate in strong GCBs was 52% whereas it was 19% in weak GCBs. In a previous study about t(14,18) occurrence in DLBCL, James and colleagues used the complementary DNA microarray-generated gene expression profile method to test 35 cases and found 7 cases with t(14,18). This group had a GCB gene expression profile which represented the strongest 35% in the GCB subset.[40] Another study by Sharon and colleagues also showed that the t(14,18) was common in the GCB subset.[41] But LPS is a linear scoring system, in which the distinction point of GCB vs. ABC is kind of arbitrary. This study is a binary distinction solely based on the "strong GCB" surrogate marker t(14,18). Hence, the project involved human DLBCL cell lines with t(14,18) as positive and negative.

Heterogeneity is the inherent feature of DLBCL. Applying therapeutic type I Rituximab and type II Obinutuzumab monoclonal antibody on 18 DLBCL cell lines could give out an integrated message for Ab-mediated direct cell killing covering a relatively wide range of DLBCL. Each of these cell lines is applied with three different concentrations. It is known that the efficacy may not be dose dependent because of the saturation of the Ab binding site[42], which makes it difficult to compare the results of an individual cell line with the rest of 17 cell lines tested here. For comprehensive understanding, these data were collected at three different doses of mAb separately

in two different groups. The results showed Obinutuzumab treatment had a stronger effect in the t+ group at 10 μg/ml, but not at 0.1 and 1 μg/ml. To some extent this accords with the GOYA clinical trial. It might be one of the reasons that in the GOYA clinical trial, O-CHOP benefitted strong GCB patients more than R-CHOP. Of note, in the GOYA clinical trial, it was a much more complicated scenario. Ab-mediated direct killing is only one aspect of mAb functions *in vivo*. There are other functions, like ADCC, ADCP, and CDC. Additionally, in clinics, the dose of Obinutuzumab is fixed at 1,000mg per patient regardless of their body surface area, which is higher than Rituximab, which has a dose of 375 mg/m^2. Whether the large fixed dose is reasonable is not known, since in the GOYA clinical trial, the side effects with Obinutuzumab were more serious than with Rituximab at this dosage. Therefore, the *in vitro* result shown here may not be reflected *in vivo*.

To explore other possibilities as to why strong GCBs benefit from Obinutuzumab plus CHOP more than Rituximab plus CHOP, and to mimic the clinical treatment situation, I focused on chemotherapy induced senescence and senolysis by Rituximab and Obinutuzumab. In clinics, traditional chemotherapy treatment is essential to achieve tumor regression in DLBCL patients.[43] The exposure of the lymphoma cells to chemotherapeutics evokes cell damage and subsequently decides the fate of these cells - to live or die. From cell damage to death is a process. Tumor cells have the capability to evade dying. With the damage inside the cell, the safeguard machinery apparatus first stops the cell cycle proliferation so as to keep the cell life alive. At some point, a stasis arises. The process for repairing non-lethal damages toward recovery is essentially therapy-induced senescence (TIS). In this project, TIS was successfully induced in 7 t+ and 6 t- cell lines by ADR. Each of the different chemotherapeutics has its own way to cause DNA damage. Depending on the duration and extent of the damage, the type of senescence can be acute or chronic.[44] It is also reported that senescence is dose dependent.[45,46] There were reports that ADR could induce cellular senescence in 1999[39,46,47] and *in vivo* patient samples by Robert and colleagues in 2002.[48] Published papers by other groups also revealed that other anticancer reagents

like alkylating agents, platinum based drugs, microtubule inhibitors, hormonal therapy, small molecular inhibitors can also induce tumor cells into senescence.[39,26]

ADR interacts with DNA by intercalation and inhibition of macromolecular biosynthesis and stabilizes the topoisomerase II complex after the DNA chain is broken, preventing the DNA double helix from being resealed and finally stops the process of replication. Once the integrity of DNA is violated, it becomes dangerous for the cells to pass it through the next generations. In the long process of evolution, an advanced system for DNA damage repair(DDR) has been developed.[49] Histone variant H2AX is a sensor protein that can be phosphorylated at the Ser-139 residue as the response of DNA double-strand breaks to form γH2AX.[50] It holds the broken chromosome ends and gives out a higher accessibility of DNA to recruit the corresponding DDR proteins.[51] It also facilitates the rejoining of DSB by anchoring broken ends through relocating the damaged site by the nucleosome.[52] At the same time, it modulates checkpoint response to arrest the cell cycle to offer a longer time for DNA repair.[53] The high expression of γH2AX after senescence induction in the t+ and t- groups was confirmed by WB in the project. Once DDR is activated, p16 will act as an inhibitor of CDK.[54] It binds with CDK4s and CDK6 to prevent phosphorylation of retinoblastoma tumor suppressor (pRB). Non-phosphorylated RB attaches to E2F, which is a group of genes encoding transcription factors(TF) for DNA synthesis, to block the cell cycle from progressing at G1/S.[54] With the cooperation of the p16/pRb pathway, chromatin structure remodeling starts up. The high expression of p16 after senescence induction in the t+ and t- groups was confirmed by WB in the project. SAHF was first explicitly reported by Narita and colleagues in 2003.[55] SAHF is a highly condensed chromosome with different densities and sizes. Inside the SAHF, there are highly expressed hypoacetylated histones and the methylation of the lysine9 of histone H3(H3K9me3) which are the anchors that enrich Heterochromatin Protein 1(HP1) protein binding.[55] SAHF includes proliferation-promoting genes and is more resistant to nuclease digestion.[55] For the maintenance of senescence state, H3K9me3 plays an essential role and the demethylating activities could override the senescence which means that continuous methyltransferase activities are needed.[57] In this project, H3K9me3 expression was significantly increased after senescence induction by WB confirmation.

SA-β-gal activity was first published as identifying senescent cells in 1995 by Dimri and colleagues. It was carried out at pH 6.0, staining the senescent cell blue with the substrate X-gal.[58] Its expression is not needed for senescence.[59] Due to the overexpression and accumulation of the endogenous lysosomal beta-galactosidase, it is widely used as a biomarker for senescent cells, with features that are easy to be detected and reliable.[59] After 5 days of treatment with ADR, 7 t+ and 6 t- cell lines showed a high activity of β-galactosidase, which were shown by SA-β-gal staining. Very few of these cell lines have been reported to be induced into senescence by ADR or other chemotherapeutics.[60,61] Furthermore, the t+ group showed higher SA-β-gal activity than the t- subgroup, which fits with our previous work reporting that primary GCB-like Eμ-myc mouse lymphoma samples transduced with Bcl2 are prone to senescence. Because it is important for combination therapy with mAb, the expression level of CD20 was measured after senescence induction in these cell lines. Lower expression of CD20 decreases the mAb efficacy.[42] CD20 was confirmed to be stable after senescence by qRT-PCR.

Another possible scenario involves the question of whether Obinutuzumab could also induce these cell lines to senescence. My laboratory previously showed that Rituximab induced B cell lymphoma to senescence with crosslinker.[28] But it is not known whether Obinutuzumab also has the senescence induction capability in DLBCL. Only one FL cell line has been reported that could be induced into senescence after 20 days of treatment with Obinutuzumab in a 3D model with C12FDG staining, but no X-gal chemical SA-β-gal activity evaluation.[62] There needs to be more exploration in this direction in DLBCL and this might be one of the reasons why Obinutuzumab has higher superiority in strong DLBCL with t(14,18).

Biologically and pathologically, TIS is a sword with two edges in cancer therapy. One aspect is beneficial. The tumor growth is stopped as the cancer cell cycles are arrested. In special cases, the cells fail to proceed with mitogen stimulation.[63] Senescent melanocytes can survive as benign nevi for years.[64] *In vivo* senescent cells may undergo phagocytosis or autophagy with secondary stress

like starvation.[65] The immune response might be activated. SASP factors including pro-inflammatory cytokines and the extracellular matrix (ECM) attract immune response and clearance. Besides the DDR pathway involved, cytoplasmic chromatin fragments (CCFs) activate the cGAS STING pathway, resulting in IFN-γ release.[66] IFN-γ activates macrophages and induces expression of the Class II major histocompatibility complex(MHC) molecule.[67] The beneficial immune network is switched on. This immune response may prolong survival rate in a mouse lymphoma model transduced with BCL2 expression in the status of TIS.[68] Senescence increases susceptibility to cell-mediated cytotoxicity in mutants of the neuroblastoma RAS viral (v-ras) oncogene homolog (NRAS) and the v-RAF murine sarcoma viral oncogene homolog B1 (BRAF) co-expressing human melanoma cells.[69] IL1α is published acting as an upstream regulator to induce NF-κB activity to promote an immune response.[70] In this project, IL1α expression after senescence in two groups was measured to be higher than untreated samples.

Conversely, this is deleterious. The immunosuppressive tissue microenvironment can be activated as well. For example, suppressive myeloid cells which have the capability to depress anti-tumor T cell reactions can be stimulated by interleukin 6 (IL-6).[71] CCL2 is shown to recruit immunosuppressive cells to promote hepatocellular carcinomas.[72] In different tumor cell types the content of SASP after senescence is heterogeneously different.[73] SASP factors including cytokines, chemokines, growth factors, and extracellular matrix constituents together might be too abundant for remodeling the tumor environment so that they would participate in cancer progression, with one example being that they could turn senescent fibroblasts into proinflammatory cells.[74] Further evidence is that macrophages are influenced to adopt an M2 phenotype that finally promotes angiogenesis and tumor development.[75] The GATA4, mTOR, and Jak2/Stat3 pathways, as well as inflammasome were found to play a role recently[76] and *in vivo* experiments showed that senescent cells stimulate ovarian tumor occurrence.[77] SASP could also induce epithelial-to-mesenchymal transition (EMT), which possibly induces increased invasiveness.[78] In this project, IL6, CCL2 expression after senescence in two groups were measured to be higher than in untreated samples.

Another area of debate is if the senescent cells are irreversible. If cell cycles are abrogated permanently, all kinds of tumors could be curable. In fact, relapse is a common feature for malignant tumors. In the experimental condition, cells expressing all the hallmarks of senescence are observed to recover from a prolonged growth arrest.[79] Work by our laboratory demonstrated cell-cycle re-entry out of robust, deep senescence based on switches of senescence-essential genes like Suv39h1:ER and JMD2C:ER.[57,23] Wu and colleagues found the frequency of escape was 1 in every 106 cells, with the suggestion that an evasion is an infrequent event.[80] Unlike a chemical reaction, the direction of the cells after senescence reversion is unsure, whether as pre-senescence phenotype analogous, or as dynamic genotypic and phenotypic change occurrence.[81,23] A MCF7 breast tumor cell colony was demonstrated to fail to reenter senescence after recovering from ADR induced senescence due to decreased intracellular ADR accumulation or attenuated DDR.[82] Our previous work showed TIS results in stemness (like CD44, CD133) reprogramming, which facilitated escape from senescence state and gaining more malignant features.[23] The process is that once damage is repaired, the cell reenters the cell cycle and continues proliferating. This overcoming of senescence with reprogramming gains more stemness characteristics for the cells, and is thus a hint that the tumor may go into relapse and become resistant to chemotherapy. Despite the proliferative recovery and disease recurrence, multiple adverse events about senescent cells have been reported. The Campisi group showed that senescent cells can cause certain chemotherapy side effects and the elimination of senescent cells can ameliorate some toxicities.[83] In this project, CD44 and CD133 expression after senescence in two groups were measured to be higher than untreated samples.

Clearance of senescent tumor cells has thus become a new approach to prevent or delay tumor relapse. After chemotherapy, senescent tumor and non-tumor cells accumulate in the body. The way to selectively eliminate senescent cells would be a complementary approach. The transgenic mouse model INK-ATTAC was developed for selectively killing $p16^{INK4}$-positive senescent cells *in vivo*.[84] Improved muscle structure and function, physical performance, and fat deposition were

observed once the senescent cells were removed.[84] However, this model cannot be used in the human body. Efforts are being put into searching for compounds that can selectively eliminate senescent cells. A few of these compounds have been reported as senolytic agents, e.g., HSP90 inhibitors, Bcl-2 family inhibitors, piperlongumine, Dasatinib/Quercetin etc. For example, Dasatinib could eliminate senescent human fat cells and quercetin would be effective against senescent human endothelial cells. A combination of the two would kill both cell types in the senescent status.[85] Navitoclax(ABT263) is a selective inhibitor of the anti-apoptotic proteins BCL-2, BCL-xL, and BCL-w. It works as a senolytic agent to kill senescent cells and could abrogate SASP response.[86]

The senolytic features of Rituximab/Obinutuzumab are thus unveiled. This project demonstrated the different capability of senolytic features between Rituximab and Obinutuzumab. Obinutuzumab had a higher senolytic capability than Rituximab in the t+ group, but not in the t- group *in vitro*. The experiment was designed using 12-carbon lipophilic moiety(C12FDG), which is a fluorescein-based substrate of SA-β-gal that is one of the best characterized markers of senescence. Once inside the cell, it produces a fluorescent product that can be well retained by the cell. It makes quantitatively measuring the senescence status by flow cytometry feasible and is reported as a method for rapid, high throughput screening of drug libraries for senolytic agents.[87] For the confirmation of senolytic activity by Rituximab/Obinutuzumab, protein expression of the previously explained well-known senescence marker H3K9me3 was measured after secondary treatment with Rituximab or Obinutuzumab for 24h. Obinutuzumab was indeed able to kill more senescent cells than Rituximab in the t+ group. And less γH2AX, the P16 expression than Rituximab afterward indicated that the proportion of senolytic activities on senescent cells was higher than the damage to non-senescent cells. Considering the limitations of the *in vitro* cell line experiment, the senolytic features of Obinutuzumab need to be further explored *in vivo*.

The Ab-mediated direct killing induced by Obinutuzumab has been published associated with lysosome induced cell death in three FL, and one DLBCL cell lines[20], as well as two chronic

lymphocytic leukemia (CLL) cell lines[88]. However, Chien and colleagues rejected the lysosomal membrane permeabilization status treated with Obinutuzumab because of the shortage of specific cathepsin B antibody, the one that was used by Alduaij and colleagues [20], which had unexpected cross-reactivity with Obinutuzumab itself.[21] Both of the groups reported that the process was a caspase-independent, actin dependent, and in a reactive oxygen species involved manner. To better understand if there is the involvement of apoptosis in the senolytic activity, the apoptosis associated pathway molecule was checked by WB. The process of apoptosis has been well studied.[89] Intrinsic and extrinsic pathways are triggered to go through programmed cell death. The changes include blebbing, cell shrinkage, nuclear fragmentation, chromatin condensation, chromosomal DNA fragmentation, and global mRNA decay. Both pathways activate caspases. One of the effector caspases is caspase-3.[90] Figure 9C shows no increase in the protein level of cleaved caspase-3 expression during the senolytic activity with Obinutuzumab. It indicates that there is no apoptosis activation during the senolytic process by Obinutuzumab in the t+ subgroup. It is consistent with published papers reporting that there is no involvement of apoptosis during LCD.[34]

Lysosensor is widely used for detecting a more accurate readout of lysosomal pH in a broad pH range (3.0-9.0).[91] It is specially engineered to become more fluorescent in acidic environments. From the results shown in Figure 9F, there was pH change during the senolytic process of Obinutuzumab in the t+. It has been well accepted since 1966 that lysosomes must keep an acidic pH to activate hydrolytic enzymes to degrade internal macromolecules.[92] Vacuolar ATPase (v-ATPase) plays a major role in maintaining this acidification by pumping protons into the lumen of the lysosome, with the consuming of the free energy of ATP hydrolysis.[93] At the same time, the secondary counterion movement like Cl^-, which is charged by chloride channels (ClC) and the transporter ClC family, has been appreciated.[94] However, the details for the quantitative measurements of the biophysical properties of lysosomes are still not clear. The pH of the lysosome was increased after secondary treatment with Obinutuzumab in the t+, meaning that the balanced acidification status of the lysosome was broken. The result might be that the

permeabilization of lysosomal membrane increased. But this still needs to be confirmed further, by exploring the possible mechanism that could account for this. Interestingly, the protein level expression of lamp l, which is on the lysosomal membrane, was relatively stable through the whole process from senescence to senolytic. And it is the same with Cathepsin B expression, which is the most important hydrolytic enzyme inside the lysosome during the senescence and senolytic activity in both subgroups. It is a complicated situation that there are different scenarios for the cathepsin family activity in the lysosome and the cytosol. It is not known if other cathepsin family members, like cathepsin D, C et al., are involved.

To summarize, the project followed the question from the deep analysis of the GOYA clinical trial as to whether, and how, senescence plays a role in the scenario that O-CHOP benefits strong GCB patients, with a detailed viewpoint into the combination therapy of CHOP chemotherapy plus mAB. To firstly induce cells to senescence by ADR then kill the senescent cells with mAb is an *in vitro* mimicking of the combination therapy strategy. In conclusion, this project demonstrates that Obinutuzumab has a higher Ab-mediated direct killing and senolytic capability than Rituximab, which might be one of the reasons that the subgroup of strong GCB patients get more benefits from O-CHOP treatment. The limitations of the project are that the data are only from cell lines *in vitro*; *in vivo* verification as well as more detailed mechanisms and other possible directions need to be further explored. By assessing ADCP, monocyte-derived macrophages which are isolated from human peripheral blood and mononuclear cells from human blood are planned to be used. Induction of CDC by mAb will be performed by testing the complement component C1q binding using ELISA. In vivo immune-reconstituted PDX mouse models are appropriate to be applied after further verification. In a further step, the molecular profiling of DLBCL under therapy must help to mark the actual qualitative and quantitative contribution to mAb-related senescence and senolysis activity. All these elements may add to the overall outcome of anti-CD20-CHOP-based chemo-immune-therapies in DLBCL.

6 References

1. Vitolo U, Trněný M, Belada D, Burke JM, Carella AM, Chua N, Abrisqueta P, Demeter J, Flinn I, Hong X, Kim WS, Pinto A, Shi Y-K, Tatsumi Y, Oestergaard MZ, Wenger M, Fingerle-Rowson G, Catalani O, Nielsen T, Martelli M, Sehn LH. Obinutuzumab or Rituximab Plus Cyclophosphamide, Doxorubicin, Vincristine, and Prednisone in Previously Untreated Diffuse Large B-Cell Lymphoma. *J Clin Oncol*. 2017;35(31):3529-3537. doi:10.1200/JCO.2017.73.3402

2. *Dorland's Illustrated Medical Dictionary*. Philadelphia : Saunders; 2000. Accessed October 28, 2020. http://archive.org/details/trent_0116404640520

3. Bardia A, Seifter E. *Johns Hopkins Patients' Guide to Lymphoma*. Jones & Bartlett Learning; 2010.

4. Krebs - Cancer in Germany. Accessed October 28, 2020. https://www.krebsdaten.de/Krebs/EN/Content/Publications/Cancer_in_Germany/cancer_in_germany_node.html

5. Alizadeh AA, Eisen MB, Davis RE, Ma C, Lossos IS, Rosenwald A, Boldrick JC, Sabet H, Tran T, Yu X, Powell JI, Yang L, Marti GE, Moore T, Jr JH, Lu L, Lewis DB, Tibshirani R, Sherlock G, Chan WC, Greiner TC, Weisenburger DD, Armitage JO, Warnke R, Levy R, Wilson W, Grever MR, Byrd JC, Botstein D, Brown PO, Staudt LM. Distinct types of diffuse large B-cell lymphoma identi®ed by gene expression pro®ling. 2000;403:9.

6. Scott DW, Wright GW, Williams PM, Lih C-J, Walsh W, Jaffe ES, Rosenwald A, Campo E, Chan WC, Connors JM, Smeland EB, Mottok A, Braziel RM, Ott G, Delabie J, Tubbs RR, Cook JR, Weisenburger DD, Greiner TC, Glinsmann-Gibson BJ, Fu K, Staudt LM, Gascoyne RD, Rimsza LM. Determining cell-of-origin subtypes of diffuse large B-cell lymphoma using gene expression in formalin-fixed paraffin-embedded tissue. *Blood*. 2014;123(8):1214-1217. doi:10.1182/blood-2013-11-536433

7. Tagawa H, Suguro M, Tsuzuki S, Matsuo K, Karnan S, Ohshima K, Okamoto M, Morishima Y, Nakamura S, Seto M. Comparison of genome profiles for identification of distinct subgroups of diffuse large B-cell lymphoma. *Blood*. 2005;106(5):1770-1777. doi:10.1182/blood-2005-02-0542

8. Motlló C, Grau J, Juncà J, Ruiz N, Mate J-L, Orna E, Navarro J-T, Vives S, Sancho J-M, Esteban D, Granada I, Feliu E, Ribera J-M, Millá F. Translocation (3;8)(q27;q24) in two cases of triple hit lymphoma. *Cancer Genet Cytogenet*. 2010;203(2):328-332. doi:10.1016/j.cancergencyto.2010.08.018

9. Nowakowski GS, Czuczman MS. ABC, GCB, and Double-Hit Diffuse Large B-Cell Lymphoma: Does Subtype Make a Difference in Therapy Selection? *Am Soc Clin Oncol*

Educ Book Am Soc Clin Oncol Annu Meet. Published online 2015:e449-457. doi:10.14694/EdBook_AM.2015.35.e449

10. Schmitz R, Wright GW, Huang DW, Johnson CA, Phelan JD, Wang JQ, Roulland S, Kasbekar M, Young RM, Shaffer AL, Hodson DJ, Xiao W, Yu X, Yang Y, Zhao H, Xu W, Liu X, Zhou B, Du W, Chan WC, Jaffe ES, Gascoyne RD, Connors JM, Campo E, Lopez-Guillermo A, Rosenwald A, Ott G, Delabie J, Rimsza LM, Tay Kuang Wei K, Zelenetz AD, Leonard JP, Bartlett NL, Tran B, Shetty J, Zhao Y, Soppet DR, Pittaluga S, Wilson WH, Staudt LM. Genetics and Pathogenesis of Diffuse Large B-Cell Lymphoma. *N Engl J Med*. 2018;378(15):1396-1407. doi:10.1056/NEJMoa1801445

11. Chapuy B, Stewart C, Dunford AJ, Kim J, Kamburov A, Redd RA, Lawrence MS, Roemer MGM, Li AJ, Ziepert M, Staiger AM, Wala JA, Ducar MD, Leshchiner I, Rheinbay E, Taylor-Weiner A, Coughlin CA, Hess JM, Pedamallu CS, Livitz D, Rosebrock D, Rosenberg M, Tracy AA, Horn H, van Hummelen P, Feldman AL, Link BK, Novak AJ, Cerhan JR, Habermann TM, Siebert R, Rosenwald A, Thorner AR, Meyerson ML, Golub TR, Beroukhim R, Wulf GG, Ott G, Rodig SJ, Monti S, Neuberg DS, Loeffler M, Pfreundschuh M, Trümper L, Getz G, Shipp MA. Molecular subtypes of diffuse large B cell lymphoma are associated with distinct pathogenic mechanisms and outcomes. *Nat Med*. 2018;24(5):679-690. doi:10.1038/s41591-018-0016-8

12. Marcus R, Sweetenham JW, Williams ME. *Lymphoma: Pathology, Diagnosis, and Treatment*. Cambridge University Press; 2013.

13. Pierpont TM, Limper CB, Richards KL. Past, Present, and Future of Rituximab—The World's First Oncology Monoclonal Antibody Therapy. *Front Oncol*. 2018;8. doi:10.3389/fonc.2018.00163

14. Kellner C, Otte A, Cappuzzello E, Klausz K, Peipp M. Modulating Cytotoxic Effector Functions by Fc Engineering to Improve Cancer Therapy. *Transfus Med Hemotherapy*. 2017;44(5):327-336. doi:10.1159/000479980

15. Butler LA, Tam CS, Seymour JF. Dancing partners at the ball: Rational selection of next generation anti-CD20 antibodies for combination therapy of chronic lymphocytic leukemia in the novel agents era. *Blood Rev*. 2017;31(5):318-327. doi:10.1016/j.blre.2017.05.002

16. Janas E, Priest R, Wilde JI, White JH, Malhotra R. Rituxan (anti-CD20 antibody)-induced translocation of CD20 into lipid rafts is crucial for calcium influx and apoptosis. *Clin Exp Immunol*. 2005;139(3):439-446. doi:10.1111/j.1365-2249.2005.02720.x

17. Mathas S, Rickers A, Bommert K, Dorken B, Mapara MY. Anti-CD20- and B-cell Receptor-mediated Apoptosis: Evidence for Shared Intracellular Signaling Pathways. :8.

18. Niederfellner G, Lammens A, Mundigl O, Georges GJ, Schaefer W, Schwaiger M, Franke A, Wiechmann K, Jenewein S, Slootstra JW, Timmerman P, Brannstrom A, Lindstrom F,

Mossner E, Umana P, Hopfner K-P, Klein C. Epitope characterization and crystal structure of GA101 provide insights into the molecular basis for type I/II distinction of CD20 antibodies. *Blood*. 2011;118(2):358-367. doi:10.1182/blood-2010-09-305847

19. Mössner E, Brünker P, Moser S, Püntener U, Schmidt C, Herter S, Grau R, Gerdes C, Nopora A, van Puijenbroek E, Ferrara C, Sondermann P, Jäger C, Strein P, Fertig G, Friess T, Schüll C, Bauer S, Dal Porto J, Del Nagro C, Dabbagh K, Dyer MJS, Poppema S, Klein C, Umaña P. Increasing the efficacy of CD20 antibody therapy through the engineering of a new type II anti-CD20 antibody with enhanced direct and immune effector cell–mediated B-cell cytotoxicity. *Blood*. 2010;115(22):4393-4402. doi:10.1182/blood-2009-06-225979

20. Alduaij W, Ivanov A, Honeychurch J, Cheadle EJ, Potluri S, Lim SH, Shimada K, Chan CHT, Tutt A, Beers SA, Glennie MJ, Cragg MS, Illidge TM. Novel type II anti-CD20 monoclonal antibody (GA101) evokes homotypic adhesion and actin-dependent, lysosome-mediated cell death in B-cell malignancies. *Blood*. 2011;117(17):4519-4529. doi:10.1182/blood-2010-07-296913

21. Chien WW, Niogret C, Jugé R, Lionnard L, Cornut-Thibaut A, Kucharczak J, Savina A, Salles G, Aouacheria A. Unexpected cross-reo183188activity of anti-cathepsin B antibodies leads to uncertainties regarding the mechanism of action of anti-CD20 monoclonal antibody GA101. *Leuk Res*. 2017;55:41-48. doi:10.1016/j.leukres.2017.01.010

22. Collado M, Blasco MA, Serrano M. Cellular senescence in cancer and aging. *Cell*. 2007;130(2):223-233. doi:10.1016/j.cell.2007.07.003

23. Milanovic M, Fan DNY, Belenki D, Däbritz JHM, Zhao Z, Yu Y, Dörr JR, Dimitrova L, Lenze D, Monteiro Barbosa IA, Mendoza-Parra MA, Kanashova T, Metzner M, Pardon K, Reimann M, Trumpp A, Dörken B, Zuber J, Gronemeyer H, Hummel M, Dittmar G, Lee S, Schmitt CA. Senescence-associated reprogramming promotes cancer stemness. *Nature*. 2017;553(7686):96-100. doi:10.1038/nature25167

24. Shay JW, Wright WE. Hayflick, his limit, and cellular ageing. *Nat Rev Mol Cell Biol*. 2000;1(1):72-76. doi:10.1038/35036093

25. Wajapeyee N, Serra RW, Zhu X, Mahalingam M, Green MR. Oncogenic BRAF Induces Senescence and Apoptosis through Pathways Mediated by the Secreted Protein IGFBP7. *Cell*. 2008;132(3):363-374. doi:10.1016/j.cell.2007.12.032

26. Ewald JA, Desotelle JA, Wilding G, Jarrard DF. Therapy-Induced Senescence in Cancer. *JNCI J Natl Cancer Inst*. 2010;102(20):1536-1546. doi:10.1093/jnci/djq364

27. Hanahan D, Weinberg RA. The Hallmarks of Cancer. *Cell*. 2000;100(1):57-70. doi:10.1016/S0092-8674(00)81683-9

28. Da britz JHM, Yu Y, Milanovic M, Scho nlein M, Rosenfeldt MT, Do rr JR, Kaufmann AM, Do rken B, Schmitt CA. CD20-Targeting Immunotherapy Promotes Cellular Senescence in B-Cell Lymphoma. *Mol Cancer Ther*. 2016;15(5):1074-1081. doi:10.1158/1535-7163.MCT-15-0627

29. Chen GG, Lai PBS, eds. *Apoptosis in Carcinogenesis and Chemotherapy: Apoptosis in Cancer*. Springer Netherlands; 2009. doi:10.1007/978-1-4020-9597-9

30. Duve C de. Lysosomes revisited. *Eur J Biochem*. 1983;137(3):391-397. doi:10.1111/j.1432-1033.1983.tb07841.x

31. Aits S, Jaattela M. Lysosomal cell death at a glance. *J Cell Sci*. 2013;126(9):1905-1912. doi:10.1242/jcs.091181

32. Sumoza-Toledo A, Penner R. TRPM2: a multifunctional ion channel for calcium signalling. *J Physiol*. 2011;589(Pt 7):1515-1525. doi:10.1113/jphysiol.2010.201855

33. Green DR, Galluzzi L, Kroemer G. Mitochondria and the autophagy-inflammation-cell death axis in organismal aging. *Science*. 2011;333(6046):1109-1112. doi:10.1126/science.1201940

34. Brojatsch J, Lima H, Palliser D, Jacobson LS, Muehlbauer SM, Furtado R, Goldman DL, Lisanti MP, Chandran K. Distinct cathepsins control necrotic cell death mediated by pyroptosis inducers and lysosome-destabilizing agents. *Cell Cycle Georget Tex*. 2015;14(7):964-972. doi:10.4161/15384101.2014.991194

35. Marcus R, Davies A, Ando K, Klapper W, Opat S, Owen C, Phillips E, Sangha R, Schlag R, Seymour JF, Townsend W, Trněný M, Wenger M, Fingerle-Rowson G, Rufibach K, Moore T, Herold M, Hiddemann W. Obinutuzumab for the First-Line Treatment of Follicular Lymphoma. *N Engl J Med*. 2017;377(14):1331-1344. doi:10.1056/NEJMoa1614598

36. Morin RD, Mendez-Lago M, Mungall AJ, Goya R, Mungall KL, Corbett RD, Johnson NA, Severson TM, Chiu R, Field M, Jackman S, Krzywinski M, Scott DW, Trinh DL, Tamura-Wells J, Li S, Firme MR, Rogic S, Griffith M, Chan S, Yakovenko O, Meyer IM, Zhao EY, Smailus D, Moksa M, Chittaranjan S, Rimsza L, Brooks-Wilson A, Spinelli JJ, Ben-Neriah S, Meissner B, Woolcock B, Boyle M, McDonald H, Tam A, Zhao Y, Delaney A, Zeng T, Tse K, Butterfield Y, Birol I, Holt R, Schein J, Horsman DE, Moore R, Jones SJM, Connors JM, Hirst M, Gascoyne RD, Marra MA. Frequent mutation of histone-modifying genes in non-Hodgkin lymphoma. *Nature*. 2011;476(7360):298-303. doi:10.1038/nature10351

37. Bolen CR, Klanova M, Trneny M, Sehn LH, He J, Tong J, Paulson JN, Kim E, Vitolo U, Rocco AD, Fingerle-Rowson G, Nielsen T, Lenz G, Oestergaard MZ. Prognostic impact of somatic mutations in diffuse large B-cell lymphoma and relationship to cell-of-origin: data

from the phase III GOYA study. *Haematologica*. 2020;105(9):2298-2307. doi:10.3324/haematol.2019.227892

38. Jing H, Kase J, Dörr JR, Milanovic M, Lenze D, Grau M, Beuster G, Ji S, Reimann M, Lenz P, Hummel M, Dörken B, Lenz G, Scheidereit C, Schmitt CA, Lee S. Opposing roles of NF-κB in anti-cancer treatment outcome unveiled by cross-species investigations. *Genes Dev*. 2011;25(20):2137-2146. doi:10.1101/gad.17620611

39. Chang BD, Broude EV, Dokmanovic M, Zhu H, Ruth A, Xuan Y, Kandel ES, Lausch E, Christov K, Roninson IB. A senescence-like phenotype distinguishes tumor cells that undergo terminal proliferation arrest after exposure to anticancer agents. *Cancer Res*. 1999;59(15):3761-3767.

40. Huang JZ, Sanger WG, Greiner TC, Staudt LM, Weisenburger DD, Pickering DL, Lynch JC, Armitage JO, Warnke RA, Alizadeh AA, Lossos IS, Levy R, Chan WC. The t(14;18) defines a unique subset of diffuse large B-cell lymphoma with a germinal center B-cell gene expression profile. *Blood*. 2002;99(7):2285-2290. doi:10.1182/blood.v99.7.2285

41. Barrans SL, Evans PAS, O'Connor SJM, Kendall SJ, Owen RG, Haynes AP, Morgan GJ, Jack AS. The t(14;18) is associated with germinal center-derived diffuse large B-cell lymphoma and is a strong predictor of outcome. *Clin Cancer Res Off J Am Assoc Cancer Res*. 2003;9(6):2133-2139.

42. Kamath AV. Translational pharmacokinetics and pharmacodynamics of monoclonal antibodies. *Drug Discov Today Technol*. 2016;21-22:75-83. doi:10.1016/j.ddtec.2016.09.004

43. Chaudhari K, Rizvi S, Syed BA. Non-Hodgkin lymphoma therapy landscape. *Nat Rev Drug Discov*. 2019;18(9):663-664. doi:10.1038/d41573-019-00051-6

44. van Deursen JM. The role of senescent cells in ageing. *Nature*. 2014;509(7501):439-446. doi:10.1038/nature13193

45. Roninson IB. Tumor cell senescence in cancer treatment. *Cancer Res*. 2003;63(11):2705-2715.

46. Meredith A-M, Dass CR. Increasing role of the cancer chemotherapeutic doxorubicin in cellular metabolism. *J Pharm Pharmacol*. 2016;68(6):729-741. doi:10.1111/jphp.12539

47. Bertheau P, Lehmann-Che J, Varna M, Dumay A, Poirot B, Porcher R, Turpin E, Plassa L-F, Roquancourt A de, Bourstyn E, Cremoux P de, Janin A, Giacchetti S, Espié M, Thé H de. p53 in breast cancer subtypes and new insights into response to chemotherapy. *The Breast*. 2013;22:S27-S29. doi:10.1016/j.breast.2013.07.005

48. te Poele RH, Okorokov AL, Jardine L, Cummings J, Joel SP. DNA damage is able to induce senescence in tumor cells in vitro and in vivo. *Cancer Res*. 2002;62(6):1876-1883.

49. Jackson SP, Bartek J. The DNA-damage response in human biology and disease. *Nature*. 2009;461(7267):1071-1078. doi:10.1038/nature08467

50. Mah L-J, El-Osta A, Karagiannis TC. γH2AX: a sensitive molecular marker of DNA damage and repair. *Leukemia*. 2010;24(4):679-686. doi:10.1038/leu.2010.6

51. Bassing CH, Alt FW. H2AX may function as an anchor to hold broken chromosomal DNA ends in close proximity. *Cell Cycle Georget Tex*. 2004;3(2):149-153. doi:10.4161/cc.3.2.689

52. Banáth JP, MacPhail SH, Olive PL. Radiation Sensitivity, H2AX Phosphorylation, and Kinetics of Repair of DNA Strand Breaks in Irradiated Cervical Cancer Cell Lines. *Cancer Res*. 2004;64(19):7144-7149. doi:10.1158/0008-5472.CAN-04-1433

53. Celeste A, Petersen S, Romanienko PJ, Fernandez-Capetillo O, Chen HT, Sedelnikova OA, Reina-San-Martin B, Coppola V, Meffre E, Difilippantonio MJ, Redon C, Pilch DR, Olaru A, Eckhaus M, Camerini-Otero RD, Tessarollo L, Livak F, Manova K, Bonner WM, Nussenzweig MC, Nussenzweig A. Genomic Instability in Mice Lacking Histone H2AX. *Science*. 2002;296(5569):922-927. doi:10.1126/science.1069398

54. Serrano M, Hannon GJ, Beach D. A new regulatory motif in cell-cycle control causing specific inhibition of cyclin D/CDK4. *Nature*. 1993;366(6456):704-707. doi:10.1038/366704a0

55. Narita M, Nũnez S, Heard E, Narita M, Lin AW, Hearn SA, Spector DL, Hannon GJ, Lowe SW. Rb-mediated heterochromatin formation and silencing of E2F target genes during cellular senescence. *Cell*. 2003;113(6):703-716. doi:10.1016/s0092-8674(03)00401-x

56. Nielsen SJ, Schneider R, Bauer UM, Bannister AJ, Morrison A, O'Carroll D, Firestein R, Cleary M, Jenuwein T, Herrera RE, Kouzarides T. Rb targets histone H3 methylation and HP1 to promoters. *Nature*. 2001;412(6846):561-565. doi:10.1038/35087620

57. Yu Y, Schleich K, Yue B, Ji S, Lohneis P, Kemper K, Silvis MR, Qutob N, van Rooijen E, Werner-Klein M, Li L, Dhawan D, Meierjohann S, Reimann M, Elkahloun A, Treitschke S, Dörken B, Speck C, Mallette FA, Zon LI, Holmen SL, Peeper DS, Samuels Y, Schmitt CA, Lee S. Targeting the Senescence-Overriding Cooperative Activity of Structurally Unrelated H3K9 Demethylases in Melanoma. *Cancer Cell*. 2018;33(2):322-336.e8. doi:10.1016/j.ccell.2018.01.002

58. Dimri GP, Lee X, Basile G, Acosta M, Scott G, Roskelley C, Medrano EE, Linskens M, Rubelj I, Pereira-Smith O. A biomarker that identifies senescent human cells in culture and in aging skin in vivo. *Proc Natl Acad Sci U S A*. 1995;92(20):9363-9367.

59. Lee BY, Han JA, Im JS, Morrone A, Johung K, Goodwin EC, Kleijer WJ, DiMaio D, Hwang ES. Senescence-associated beta-galactosidase is lysosomal beta-galactosidase. *Aging Cell*. 2006;5(2):187-195. doi:10.1111/j.1474-9726.2006.00199.x

60. Clozel T, Yang S, Elstrom RL, Tam W, Martin P, Kormaksson M, Banerjee S, Vasanthakumar A, Culjkovic B, Scott DW, Wyman S, Leser M, Shaknovich R, Chadburn A, Tabbo F, Godley LA, Gascoyne RD, Borden KL, Inghirami G, Leonard JP, Melnick A, Cerchietti L. Mechanism-Based Epigenetic Chemosensitization Therapy of Diffuse Large B Cell Lymphoma. *Cancer Discov*. 2013;3(9):1002-1019. doi:10.1158/2159-8290.CD-13-0117

61. Trabucco SE, Gerstein RM, Evens AM, Bradner JE, Shultz LD, Greiner DL, Zhang H. Inhibition of bromodomain proteins for the treatment of human diffuse large B-cell lymphoma. *Clin Cancer Res Off J Am Assoc Cancer Res*. 2015;21(1):113-122. doi:10.1158/1078-0432.CCR-13-3346

62. Decaup E, Jean C, Laurent C, Gravelle P, Fruchon S, Capilla F, Marrot A, Al Saati T, Frenois F-X, Laurent G, Klein C, Varoqueaux N, Savina A, Fournié J-J, Bezombes C. Anti-tumor activity of obinutuzumab and rituximab in a follicular lymphoma 3D model. *Blood Cancer J*. 2013;3(8):e131. doi:10.1038/bcj.2013.32

63. Stein GH, Drullinger LF, Robetorye R, Pereira-Smith OM, Smith JR. Senescent cells fail to express the CDC2 gene in response to mitogen stimulation. *Proc Natl Acad Sci U S A*. 1992;88:11012-11016. doi:10.1073/pnas.88.24.11012

64. Michaloglou C, Vredeveld LCW, Soengas MS, Denoyelle C, Kuilman T, van der Horst CMAM, Majoor DM, Shay JW, Mooi WJ, Peeper DS. BRAFE600-associated senescence-like cell cycle arrest of human naevi. *Nature*. 2005;436(7051):720-724. doi:10.1038/nature03890

65. Gerland L-M, Peyrol S, Lallemand C, Branche R, Magaud J-P, Ffrench M. Association of increased autophagic inclusions labeled for beta-galactosidase with fibroblastic aging. *Exp Gerontol*. 2003;38(8):887-895. doi:10.1016/s0531-5565(03)00132-3

66. Dou Z, Ghosh K, Vizioli MG, Zhu J, Sen P, Wangensteen KJ, Simithy J, Lan Y, Lin Y, Zhou Z, Capell BC, Xu C, Xu M, Kieckhaefer JE, Jiang T, Shoshkes-Carmel M, Ahasan Al Tanim KM, Barber GN, Seykora JT, Millar SE, Kaestner KH, Garcia BA, Adams PD, Berger SL. Cytoplasmic chromatin triggers inflammation in senescence and cancer. *Nature*. 2017;550(7676):402-406. doi:10.1038/nature24050

67. Butticè G, Miller J, Wang L, Smith BD. Interferon-γ Induces Major Histocompatibility Class II Transactivator (CIITA) That Mediates Collagen Repression and Major Histocompatibility Class II Activation by Human Aortic Smooth Muscle Cells. *Circ Res*. 2006;98(4):472-479. doi:10.1161/01.RES.0000204725.46332.97

68. Schmitt CA, Fridman JS, Yang M, Lee S, Baranov E, Hoffman RM, Lowe SW. A Senescence Program Controlled by p53 and p16INK4a Contributes to the Outcome of Cancer Therapy. *Cell*. 2002;109(3):335-346. doi:10.1016/S0092-8674(02)00734-1

69. Petti C, Molla A, Vegetti C, Ferrone S, Anichini A, Sensi M. Coexpression of NRASQ61R and BRAFV600E in human melanoma cells activates senescence and increases susceptibility to cell-mediated cytotoxicity. *Cancer Res*. 2006;66(13):6503-6511. doi:10.1158/0008-5472.CAN-05-4671

70. Su Y, Xu C, Sun Z, Liang Y, Li G, Tong T, Chen J. S100A13 promotes senescence-associated secretory phenotype and cellular senescence via modulation of non-classical secretion of IL-1α. *Aging*. 2019;11(2):549-572. doi:10.18632/aging.101760

71. Ruhland MK, Loza AJ, Capietto A-H, Luo X, Knolhoff BL, Flanagan KC, Belt BA, Alspach E, Leahy K, Luo J, Schaffer A, Edwards JR, Longmore G, Faccio R, DeNardo DG, Stewart SA. Stromal senescence establishes an immunosuppressive microenvironment that drives tumorigenesis. *Nat Commun*. 2016;7(1):11762. doi:10.1038/ncomms11762

72. Eggert T, Wolter K, Ji J, Ma C, Yevsa T, Klotz S, Medina-Echeverz J, Longerich T, Forgues M, Reisinger F, Heikenwalder M, Wang XW, Zender L, Greten TF. Distinct Functions of Senescence-Associated Immune Responses in Liver Tumor Surveillance and Tumor Progression. *Cancer Cell*. 2016;30(4):533-547. doi:10.1016/j.ccell.2016.09.003

73. Hernandez-Segura A, Jong TV de, Melov S, Guryev V, Campisi J, Demaria M. Unmasking Transcriptional Heterogeneity in Senescent Cells. *Curr Biol*. 2017;27(17):2652-2660.e4. doi:10.1016/j.cub.2017.07.033

74. Coppé J-P, Desprez P-Y, Krtolica A, Campisi J. The Senescence-Associated Secretory Phenotype: The Dark Side of Tumor Suppression. *Annu Rev Pathol Mech Dis*. 2010;5(1):99-118. doi:10.1146/annurev-pathol-121808-102144

75. Kelly J, Ali Khan A, Yin J, Ferguson TA, Apte RS. Senescence regulates macrophage activation and angiogenic fate at sites of tissue injury in mice. *J Clin Invest*. 2007;117(11):3421-3426. doi:10.1172/JCI32430

76. Borodkina AV, Deryabin PI, Giukova AA, Nikolsky NN. "Social Life" of Senescent Cells: What Is SASP and Why Study It? *Acta Naturae*. 2018;10(1):4-14.

77. Mikuła-Pietrasik J, Sosińska P, Naumowicz E, Maksin K, Piotrowska H, Woźniak A, Szpurek D, Książek K. Senescent peritoneal mesothelium induces a pro-angiogenic phenotype in ovarian cancer cells in vitro and in a mouse xenograft model in vivo. *Clin Exp Metastasis*. 2016;33(1):15-27. doi:10.1007/s10585-015-9753-y

78. Ohanna M, Cheli Y, Bonet C, Bonazzi VF, Allegra M, Giuliano S, Bille K, Bahadoran P, Giacchero D, Lacour JP, Boyle GM, Hayward NF, Bertolotto C, Ballotti R. Secretome

from senescent melanoma engages the STAT3 pathway to favor reprogramming of naive melanoma towards a tumor-initiating cell phenotype. *Oncotarget*. 2013;4(12):2212-2224. doi:10.18632/oncotarget.1143

79. Sabisz M, Skladanowski A. Cancer stem cells and escape from drug-induced premature senescence in human lung tumor cells: implications for drug resistance and in vitro drug screening models. *Cell Cycle Georget Tex*. 2009;8(19):3208-3217. doi:10.4161/cc.8.19.9758

80. Roberson RS, Kussick SJ, Vallieres E, Chen S-YJ, Wu DY. Escape from therapy-induced accelerated cellular senescence in p53-null lung cancer cells and in human lung cancers. *Cancer Res*. 2005;65(7):2795-2803. doi:10.1158/0008-5472.CAN-04-1270

81. Yang L, Fang J, Chen J. Tumor cell senescence response produces aggressive variants. *Cell Death Discov*. 2017;3:17049. doi:10.1038/cddiscovery.2017.49

82. Elmore LW, Di X, Dumur C, Holt SE, Gewirtz DA. Evasion of a single-step, chemotherapy-induced senescence in breast cancer cells: implications for treatment response. *Clin Cancer Res Off J Am Assoc Cancer Res*. 2005;11(7):2637-2643. doi:10.1158/1078-0432.CCR-04-1462

83. Demaria M, O'Leary MN, Chang J, Shao L, Liu S, Alimirah F, Koenig K, Le C, Mitin N, Deal AM, Alston S, Academia EC, Kilmarx S, Valdovinos A, Wang B, de Bruin A, Kennedy BK, Melov S, Zhou D, Sharpless NE, Muss H, Campisi J. Cellular Senescence Promotes Adverse Effects of Chemotherapy and Cancer Relapse. *Cancer Discov*. 2017;7(2):165-176. doi:10.1158/2159-8290.CD-16-0241

84. Baker DJ, Wijshake T, Tchkonia T, LeBrasseur NK, Childs BG, van de Sluis B, Kirkland JL, van Deursen JM. Clearance of p16Ink4a-positive senescent cells delays ageing-associated disorders. *Nature*. 2011;479(7372):232-236. doi:10.1038/nature10600

85. Zhu Y, Tchkonia T, Pirtskhalava T, Gower AC, Ding H, Giorgadze N, Palmer AK, Ikeno Y, Hubbard GB, Lenburg M, O'Hara SP, LaRusso NF, Miller JD, Roos CM, Verzosa GC, LeBrasseur NK, Wren JD, Farr JN, Khosla S, Stout MB, McGowan SJ, Fuhrmann-Stroissnigg H, Gurkar AU, Zhao J, Colangelo D, Dorronsoro A, Ling YY, Barghouthy AS, Navarro DC, Sano T, Robbins PD, Niedernhofer LJ, Kirkland JL. The Achilles' heel of senescent cells: from transcriptome to senolytic drugs. *Aging Cell*. 2015;14(4):644-658. doi:10.1111/acel.12344

86. Chang J, Wang Y, Shao L, Laberge R-M, Demaria M, Campisi J, Janakiraman K, Sharpless NE, Ding S, Feng W, Luo Y, Wang X, Aykin-Burns N, Krager K, Ponnappan U, Hauer-Jensen M, Meng A, Zhou D. Clearance of senescent cells by ABT263 rejuvenates aged hematopoietic stem cells in mice. *Nat Med*. 2016;22(1):78-83. doi:10.1038/nm.4010

87. Fuhrmann-Stroissnigg H, Santiago FE, Grassi D, Ling Y, Niedernhofer LJ, Robbins PD. SA-β-Galactosidase-Based Screening Assay for the Identification of Senotherapeutic Drugs. *J Vis Exp JoVE*. 2019;(148). doi:10.3791/58133

88. Jak M, van Bochove GGW, Reits EA, Kallemeijn WW, Tromp JM, Umana P, Klein C, van Lier RAW, van Oers MHJ, Eldering E. CD40 stimulation sensitizes CLL cells to lysosomal cell death induction by type II anti-CD20 mAb GA101. *Blood*. 2011;118(19):5178-5188. doi:10.1182/blood-2011-01-331702

89. Elmore S. Apoptosis: a review of programmed cell death. *Toxicol Pathol*. 2007;35(4):495-516. doi:10.1080/01926230701320337

90. D'Arcy MS. Cell death: a review of the major forms of apoptosis, necrosis and autophagy. *Cell Biol Int*. 2019;43(6):582-592. doi:10.1002/cbin.11137

91. Diwu Z, Chen CS, Zhang C, Klaubert DH, Haugland RP. A novel acidotropic pH indicator and its potential application in labeling acidic organelles of live cells. *Chem Biol*. 1999;6(7):411-418. doi:10.1016/s1074-5521(99)80059-3

92. De Duve C, Wattiaux R. Functions of lysosomes. *Annu Rev Physiol*. 1966;28:435-492. doi:10.1146/annurev.ph.28.030166.002251

93. Ohkuma S, Moriyama Y, Takano T. Identification and characterization of a proton pump on lysosomes by fluorescein-isothiocyanate-dextran fluorescence. *Proc Natl Acad Sci U S A*. 1982;79(9):2758-2762. doi:10.1073/pnas.79.9.2758

94. Steinberg BE, Huynh KK, Brodovitch A, Jabs S, Stauber T, Jentsch TJ, Grinstein S. A cation counterflux supports lysosomal acidification. *J Cell Biol*. 2010;189(7):1171-1186. doi:10.1083/jcb.200911083

7 Eidesstattliche Versicherung

„Ich, Xinxin Sun, versichere an Eides statt durch meine eigenhändige Unterschrift, dass ich die vorgelegte Dissertation mit dem Thema: Antikörper-vermittelte direkte Abtötung und senolytische Kapazität zwei monoklonaler Anti-CD20-Antikörper in humanen diffus großzelligen B-Zell-Lymphom-Zelllinien. Antibody-mediated direct killing and senolytic capacity of two distinct anti-CD20 monoclonal antibodies in human diffuse large B-cell lymphoma cell lines selbstständig und ohne nicht offengelegte Hilfe Dritter verfasst und keine anderen als die angegebenen Quellen und Hilfsmittel genutzt habe.
Alle Stellen, die wörtlich oder dem Sinne nach auf Publikationen oder Vorträgen anderer Autoren/innen beruhen, sind als solche in korrekter Zitierung kenntlich gemacht. Die Abschnitte zu Methodik (insbesondere praktische Arbeiten, Laborbestimmungen, statistische Aufarbeitung) und Resultaten (insbesondere Abbildungen, Graphiken und Tabellen) werden von mir verantwortet.

[Für den Fall, dass Sie die Forschung für Ihre Promotion ganz oder teilweise in Gruppenarbeit durchgeführt haben:] Ich versichere ferner, dass ich die in Zusammenarbeit mit anderen Personen generierten Daten, Datenauswertungen und Schlussfolgerungen korrekt gekennzeichnet und meinen eigenen Beitrag sowie die Beiträge anderer Personen korrekt kenntlich gemacht habe (siehe Anteilserklärung). Texte oder Textteile, die gemeinsam mit anderen erstellt oder verwendet wurden, habe ich korrekt kenntlich gemacht.

Meine Anteile an etwaigen Publikationen zu dieser Dissertation entsprechen denen, die in der untenstehenden gemeinsamen Erklärung mit dem/der Erstbetreuer/in, angegeben sind. Für sämtliche im Rahmen der Dissertation entstandenen Publikationen wurden die Richtlinien des ICMJE (International Committee of Medical Journal Editors; www.icmje.og) zur Autorenschaft eingehalten. Ich erkläre ferner, dass ich mich zur Einhaltung der Satzung der Charité – Universitätsmedizin Berlin zur Sicherung Guter Wissenschaftlicher Praxis verpflichte.

Weiterhin versichere ich, dass ich diese Dissertation weder in gleicher noch in ähnlicher Form bereits an einer anderen Fakultät eingereicht habe.

Die Bedeutung dieser eidesstattlichen Versicherung und die strafrechtlichen Folgen einer unwahren eidesstattlichen Versicherung (§§156, 161 des Strafgesetzbuches) sind mir bekannt und bewusst.“

Datum Unterschrift

8 Curriculum Vitae

For data protection reasons, my curriculum vitae will not be published in the electronic version of my work.

9 List of publications

1.**SUN Xinxin**, HUANG Dongmei. Efficacy of taxane-related chemotherapy with nedaplatin and other platinum-based drug regimens in Patients with advanced gynecological neoplasms. Chinese Journal of Clinical Oncology,2012,39(11):799-802.

2. **SUN Xinxin**, HUANG Dongmei, LIU Yuling. Comparative study of toxicity of chemotherapy regimen containing platinum combined with taxanes in patients with gynecological neoplasms. Chong Qing Medicine, 2012,41(22):2383-2385.

3.LAN lan, HUANG Dongmei, DENG Kehong, WANG Chunping, **SUN Xinxin**, WANG Fang, WAN Shi, MAO Meng. Clinical analysis of diagnosis and treatment of high-level cervical intraepithelial neoplasia. Journal of Practical Obstetrics and Gynecology, 2013,29(2):140-144.

4.XU Jing, HUANG Dongmei, **SUN Xinxin**.Clinical analysis of two dosage regimens of plus carboplatin intravenous chemotherapy in the treatment of advanced epithelial ovarian cancer. Journal of Chongqing Medical University, 2013, (3):409-411.

10 Acknowledgement

I would first thank Prof. Clemens Schmitt for providing the topic, the introduction to the process of scientific work, and logical ideas, especially for his continuous support of the project. Second, I would like to thank Prof. Michael Hummel who gave me suggestions on the project. And Thanks to the scientists in the working group led by Prof. Schmitt for their help in learning the applying experimental techniques in the project. Third, I would like to thank Dr. Soyoung Lee for giving me advices on the data and thesis revising. Last, I would like to thank my husband Bing Liu and daughters Chang Liu, Xu Liu and other family members for their unconditional support during my entire doctoral period.

11 Statistician certificate

CHARITÉ

CharitéCentrum für Human- und Gesundheitswissenschaften

Charité | Campus Charité Mitte | 10117 Berlin

Institut für Biometrie und klinische Epidemiologie (iBikE)

Direktor: Prof. Dr. Geraldine Rauch

Postanschrift:
Charitéplatz 1 | 10117 Berlin
Besucheranschrift:
Reinhardtstr. 58 | 10117 Berlin

Tel. +49 (0)30 450 562171
geraldine.rauch@charite.de
https://biometrie.charite.de/

Name, Vorname: Sun, Xinxin

Emailadresse: xinxin.sun@charite.de

Matrikelnummer: [redacted]

PromotionsbetreuerIn: Prof. Dr. med. Clemens Schmitt

Promotionsinstitution/Klinik: Medizinischen Klinik m.S. Hämatologie, Onkologie und Tumorimmunologie CVK

Bescheinigung

Hiermit bescheinige ich, dass Frau Xinxin Sun innerhalb der Service Unit Biometrie des Instituts für Biometrie und klinische Epidemiologie (iBikE) bei mir eine statistische Beratung zu einem Promotionsvorhaben wahrgenommen hat. Folgende Beratungstermine wurden wahrgenommen:

- Termin 1: *17.11.2020*

Folgende wesentliche Ratschläge hinsichtlich einer sinnvollen Auswertung und Interpretation der Daten wurden während der Beratung erteilt:

- Überprüfung der Normalverteilung mithilfe eines Tests oder graphisch (vorzugsweise graphisch), dann dementsprechend t-test für abhängige Stichproben oder Wilcoxon-Test wählen
- Graphische Darstellung

Diese Bescheinigung garantiert nicht die richtige Umsetzung der in der Beratung gemachten Vorschläge, die korrekte Durchführung der empfohlenen statistischen Verfahren und die richtige Darstellung und Interpretation der Ergebnisse. Die Verantwortung hierfür obliegt allein dem Promovierenden. Das Institut für Biometrie und klinische Epidemiologie übernimmt hierfür keine Haftung.

Datum: 17.11.2020

Name des Beraters/ der Beraterin: Pimrapat Gebert

[redacted]

Unterschrift BeraterIn, Institutsstempel

CHARITÉ
UNIVERSITÄTSMEDIZIN BERLIN
Institut für Biometrie und
Klinische Epidemiologie
Campus Charité Mitte
Charitéplatz 1 | D-10117 Berlin
Sitz: Reinhardtstr. 58